JGP Journal of General Physiology

RESEARCH ARTICLE

Phosphorylation of the ryanodine receptor 2 at serine 2030 is required for a complete β-adrenergic response

Duilio M. Potenza[1], Radoslav Janicek[1], Miguel Fernandez-Tenorio[1], Emmanuel Camors[3], Roberto Ramos-Mondragón[3], Héctor H. Valdivia[2,3], and Ernst Niggli[1]

During physical exercise or stress, the sympathetic system stimulates cardiac contractility via β-adrenergic receptor (β-AR) activation, resulting in protein kinase A (PKA)–mediated phosphorylation of the cardiac ryanodine receptor RyR2. PKA-dependent "hyperphosphorylation" of the RyR2 channel has been proposed as a major impairment that contributes to progression of heart failure. However, the sites of PKA phosphorylation and their phosphorylation status in cardiac diseases are not well defined. Among the known RyR2 phosphorylation sites, serine 2030 (S2030) remains highly controversial as a site of functional impact. We examined the contribution of RyR2-S2030 to Ca^{2+} signaling and excitation–contraction coupling (ECC) in a transgenic mouse with an ablated RyR2-S2030 phosphorylation site (RyR2-S2030A$^{+/+}$). We assessed ECC gain by using whole-cell patch–clamp recordings and confocal Ca^{2+} imaging during β-ARs stimulation with isoproterenol (Iso) and consistent SR Ca^{2+} loading and L-type Ca^{2+} current (I_{Ca}) triggering. Under these conditions, ECC gain is diminished in mutant compared with WT cardiomyocytes. Resting Ca^{2+} spark frequency (CaSpF) with Iso is also reduced by mutation of S2030. In permeabilized cells, when SR Ca^{2+} pump activity is kept constant (using 2D12 antibody against phospholamban), cAMP does not change CaSpF in S2030A$^{+/+}$ myocytes. Using Ca^{2+} spark recovery analysis, we found that mutant RyR Ca^{2+} sensitivity is not enhanced by Iso application, contrary to WT RyRs. Furthermore, ablation of RyR2-S2030 prevents acceleration of Ca^{2+} waves and increases latency to the first spontaneous Ca^{2+} release after a train of stimulations during Iso treatment. Together, these results suggest that phosphorylation at S2030 may represent an important step in the modulation of RyR2 activity during β-adrenergic stimulation and a potential target for the development of new antiarrhythmic drugs.

Introduction

In heart muscle cells, Ca^{2+} release from the SR via cardiac ryanodine receptor type 2 (RyR2) channels is a cornerstone of excitation–contraction coupling (ECC). During each heartbeat, a transient SR Ca^{2+} release amplifies Ca^{2+} influx via L-type Ca^{2+} channels (LTCCs) by means of the CICR mechanism. RyR2s are thought to be involved, not only in the regulation of cardiac Ca^{2+} signaling but also in the malfunctioning of this mechanism during several cardiac diseases (e.g., via posttranslational RyR2 modifications or RyR2 mutations). Besides this triggered and precisely coordinated Ca^{2+} release, RyR2s can open accidentally during diastole, giving rise to spontaneous Ca^{2+} sparks or even Ca^{2+} waves, which constitute an SR Ca^{2+} leak and are thought to be proarrhythmic via generation of diastolic delayed afterdepolarizations (DADs).

RyR phosphorylation has been recognized as a modulator of RyR function during both systole and diastole. Furthermore, RyR2 ("hyper")-phosphorylation after chronic β-adrenergic receptor (β-AR) stimulation has been implicated in Ca^{2+} signaling disturbances during heart failure (HF; Marx et al., 2000). RyR2 phosphorylation may also acutely precipitate stress-induced arrhythmias (e.g., catecholaminergic polymorphic ventricular tachycardias [CPVTs] in patients harboring RyR2 mutations; George et al., 2007).

Within the large tetrameric RyR2 macromolecular complex, several phosphorylation sites have been identified, often in strategic proximity to protein kinases and phosphatases scaffolded to the RyR. Both coordinate the extent of phosphorylation for specific sites, such as during β-AR activation. Among the identi-

[1]Department of Physiology, University of Bern, Bern, Switzerland; [2]Department of Medicine, Wisconsin Institutes for Medical Research, University of Wisconsin, Madison, WI; [3]Center for Arrhythmia Research, Department of Medicine, University of Michigan, Ann Arbor, MI.

Correspondence to Ernst Niggli: niggli@pyl.unibe.ch; E. Camor's present address is Department of Pediatrics, University of Tennessee Health Science Center, Memphis, TN.

fied phosphorylation sites, three have been found to change RyR2 activity, and their impact on cardiac function has been partly characterized over the past years: serine 2808 (S2808), S2814, and S2030 (Witcher et al., 1991; Wehrens et al., 2004; Xiao et al., 2005). However, the precise functional consequences of their phosphorylation are controversial (Bers, 2012; Valdivia, 2012). To examine the role of RyR2 phosphorylation of these specific sites from the molecular level to the complexity of an intact organism, transgenic mice have been created for the S2808 and S2814 sites, which are also referred to as the "phosphorylation hotspot." Either the modified RyR2 channels in these mice lack the phosphorylation site (S2808A, S2814A) or the animals are engineered to mimic a constitutively phosphorylated site (S2808D and S2814D).

S2808A mice appeared to exhibit a minor phenotype on the level of cellular Ca^{2+} signaling, even during β-AR stimulation (Ullrich et al., 2012). These transgenic mice show partial HF cardioprotection after myocardial infarction in some studies (Wehrens et al., 2006), but not in others, (Zhang et al., 2012), possibly depending on the particular infarct model or other experimental differences (for review, see Niggli et al., 2013). Myocytes isolated from constitutively phosphorylated S2808D mice show elevated Ca^{2+} spark frequencies and reduced SR–Ca^{2+} content, and the hearts develop an age-dependent hypertrophy (Shan et al., 2010). Mice harboring mutations of the RyR2-S2814 site generally have a more pronounced phenotype. The RyR2-S2814A mutation presents with slowed progression of HF and cardiac remodeling after transverse aortic constriction, and the isolated cells exhibited fewer Ca^{2+} waves and a reduced SR Ca^{2+} leak (Respress et al., 2012). Mice with the S2814D mutation have a propensity for ventricular arrhythmias and sudden cardiac death when stressed (van Oort et al., 2010).

Regarding the more recently discovered S2030 phosphorylation site, the information available in the literature is still rather scarce. This site was found to be phosphorylated by PKA, but to an appreciable extent only after β-AR stimulation (Xiao et al., 2005). For functional studies, phosphomutant RyR2-S2030A and S2030D channels have been expressed in HEK293 cells (Xiao et al., 2007). In lipid bilayer experiments, reconstituted S2030D channels were found to have a much higher sensitivity for the SR luminal Ca^{2+} concentration than the S2030A variant, whereas the S2030A modification showed a blunted response to PKA.

To define the implications of the RyR2-S2030 site in the native cellular environment of the channel, we engineered a RyR2-S2030A$^{+/+}$ knock-in mouse in which the RyR2 channel cannot be phosphorylated at the S2030 residue, in analogy to the previously established transgenic models for other RyR2 phosphorylation sites. Using cardiomyocytes isolated from these animals, we examined ECC and Ca^{2+} signaling by combining laser-scanning confocal Ca^{2+} imaging with a variety of experimental approaches. Our data suggest that the S2030 site contributes considerably to the molecular and cellular response during β-AR stimulation.

Materials and methods

RyR2-S2030A$^{+/+}$ mouse line

All mice were handled according to the *Guide for the Care and Handling of Laboratory Animals* published by the National Institutes of Health and National Research Council of the National Academy of Sciences and with permission of the State Veterinary Administration and according to Swiss Federal Animal protection law (permit BE 108/15). The murine *RyR2* gene sequence was derived from 129Sv CITB BAC library (Thermo Fisher Scientific). The S2030A mutation (serine-to-alanine substitution) and NEO selection cassette were introduced into a plasmid by recombination engineering. The mutation was inserted to generate a new specific recognition sequence for the SalI restriction enzyme. The vector was electroporated into mouse R1 embryonic stem cells, and the clones were selected for growth on G418. 480 NEO clones were expanded and genomic DNA isolated from each clone. Southern blot and DNA sequence analysis identified the clones that had integrated the S2030A substitution and the NEO cassette by homologous recombination. These clones were injected into C57BL/6 blastocysts. Chimeric founders were backcrossed to C57BL/6 mice twice, and the agouti pups carrying the RyR2-S2030A$^{+/+}$ mutation were identified by Southern blot and PCR. Heterozygous mice (RyR2-S2030A$^{+/-}$) were then crossed with 129Sv WT mice and maintained in this genetic background for multiple generations.

The genotyping was performed on mouse tail genomic DNA with primers that detect a sequence of 325 bp (forward primer: 5′-CAGTTTTTAATGAGATG-3′; reverse primer: 5′-AATAACCAT GAACTCTGT-3′). The detection of the homozygous (S2030A$^{+/+}$) or the WT (S2030A$^{-/-}$) alleles was possible after digestion of the PCR amplified sequence with SalI.

The ratio of heart weight (HW) to body weight (BW) was measured and used as an index of hypertrophy. Specifically, the BW of RyR2-S2030A$^{+/+}$ and age-matched WT mice (~5 mo old), were measured before the heparin injection. Hearts trimmed of extracardiac tissue were weighed immediately after surgical removal and prior cannulation. Fig. S1 shows that S2030A$^{+/+}$ mice had a significantly higher HW/BW ratio.

Transthoracic echocardiography was performed with a Vevo 2100 system with a 22–55 MHz transducer (MS550D; Visual Sonics), as described previously (Benkusky et al., 2007). In brief, mice ($n = 7$ for both WT and S2030A$^{+/+}$) were anesthetized by 5% isoflurane inhalation and maintained in the anesthetized state by 1.5–2% isoflurane. Two-dimensionally guided B-mode images of the left ventricle (LV) were acquired at the tip of the papillary muscles. LV volume was measured during systole and diastole, stroke volume, and ejection fraction. The fractional shortening was calculated by the formula [(LV diameter diastole − LV diameter systole)/LV diameter diastole] × 100.

Isolation of ventricular cardiomyocytes

To reduce variability between animals, the study was performed only in male mice. Ventricular myocytes were isolated from RyR2-S2030A$^{+/+}$ male mice and WT littermates according to an established protocol (Louch et al., 2011). Briefly, 4- to 8-mo-old mice were euthanized by cervical dislocation and the hearts were excised, cannulated and retrogradely perfused on a custom made Langendorff system. 100 µl of heparin (2,000 units/ml) was injected 10 min before the heart removal to prevent blood coagulation. To isolate the cardiomyocytes, hearts were perfused at 37°C for 15 min with a Ca^{2+}-free solution composed of (in mmol/

liter) 140 NaCl, 5.4 KCl, 1.1 $MgCl_2$, 10 HEPES, 1 NaH_2PO_4, and 10 glucose (pH 7.4, adjusted with NaOH). Cells were enzymatically dissociated using a cocktail of collagenase type II (160 U/ml, Worthington) and protease type XIV (0.21 U/ml; Sigma). After isolation, ventricular myocytes were kept at room temperature in a solution containing 250 µmol/liter Ca^{2+} and used within 6 h.

Experimental solutions

During the experiments, cardiomyocytes were perfused with a bath solution containing (in mmol/liter) 140 NaCl, 5 HEPES, 1.1 $MgCl_2$, 5.4 KCl, 10 glucose, and 1.8 $CaCl_2$ (pH 7.4, adjusted with NaOH). For the patch-clamp experiments, the cells were perfused with a solution containing (in mmol/liter) 140 NaCl, 5 HEPES, 1.1 $MgCl_2$, 5.4 KCl, 10 glucose, 0.5 $BaCl_2$, 1 CsCl, and 1.8 $CaCl_2$ (pH 7.4).

A rapid-switch, gravity-driven superfusion device was used to change experimental solutions and expose cells to isoproterenol (Iso, 100 nmol/liter) for the β-adrenergic pathway stimulation, to ryanodine (50 nmol/liter) for repetitive sparks measurements, and to caffeine (10 mmol/liter) to assess Ca^{2+} content of the SR. Iso was prepared for every experiment from a 10 mmol/liter stock, and a fresh aliquot of ryanodine was used for each experimental day. The patch pipette solution contained (in mmol/liter) 120 CsAsp, 8 NaCl, 20 TEA-Cl, 5 $MgCl_2$, 4 K_2ATP, 5 HEPES, and 0.1 K_5-fluo-3 (pH 7.2, adjusted with CsOH).

Myocytes were permeabilized by exposure to β-escin (0.005%) for 1 min. The solution used to permeabilize the cells was composed of (in mmol/liter) 100 K-Asp, 20 KCl, 3.7 $MgCl_2$, 0.5 EGTA, 10 HEPES, and 0.005% β-escin (pH 7.2). Permeabilized ventricular myocytes were then resuspended in an escin-free solution adjusted for Ca^{2+} spark and Ca^{2+} wave detection. For Ca^{2+} spark measurements, the solution containing fluo-3 pentapotassium salt (50 µmol/liter) was composed of (in mmol/liter) 120 K-Asp, 3 K_2ATP, 0.5 EGTA, 10 HEPES, and 10 phosphocreatine and 5 U/ml creatine phosphokinase, 3 $MgCl_2$, 50 nmol/liter (free) Ca^{2+}, and 8% wt/vol dextran (to prevent osmotic swelling). For the measurement of Ca^{2+} waves, the free [Ca^{2+}] was fixed to 0.6 µmol/liter, to generate a high frequency of Ca^{2+} release events. Free Ca^{2+} concentrations were measured and adjusted with a NanoDrop ND-3300 fluorospectrometer (Thermo Fisher Scientific) and Indo-1 pentapotassium salt as a ratiometric Ca^{2+} indicator (10 µmol/liter; Biotium). Where indicated, permeabilized myocytes were treated with cyclic adenosine monophosphate (cAMP; 5 µmol/liter) for 5–10 min and with the antibody-binding fragment (Fab; 100 µg/ml) of the monoclonal phospholamban (PLB) antibody 2D12 (Thermo Fisher Scientific) for 15 min. Unless otherwise indicated, chemicals were purchased from MilliporeSigma. Experiments were performed at room temperature (21°C).

Generation of the 2D12 Fab

To facilitate its penetration into and its distribution inside permeabilized myocytes, the 2D12 PLB antibody (1 mg/ml) was fragmented by using a commercial kit (Fab Preparation Kit, no. 4468; Thermo Fisher Scientific; Chan et al., 2015). In brief, the kit uses papain immobilized on agarose resin to digest the antibody, producing ∼50 kD Fab and crystallizable fragments. After digestion, the Fab was purified from undigested IgG and Fc. Sodium azide was present in the 2D12 antibody storage solution. Because this solution may be toxic to cells, it was dialyzed with a molecular weight cutoff (DiaEasy Dialyzer MWCO 12–14 kD; BioVision). To assess digestion completion, the digested fragments were run on nonreducing SDS-PAGE. Protein concentration was measured by absorbance at 280 nm (NanoDrop Spectrophotometer).

Electrophysiological recordings

For electrophysiological measurements, L-type Ca^{2+} current (I_{Ca}) was recorded from ventricular myocytes with the patch-clamp technique in the whole-cell configuration with an Axopatch 200 amplifier (Axon Instruments). Pipettes with ∼1.5-µm tip diameter and 1.5–3 MΩ resistance were pulled from borosilicate glass micropipettes (no. G150F-3; Warner Instruments) with a DMZ puller (Zeitz Instruments). Cells were allowed 4–5 min for dialysis with the pipette solution. Membrane currents were recorded by using custom-written software developed by us in LabView (National Instruments), and the data were analyzed with IgorPro software (version 6.34A; WaveMetrics). Cells were held at a potential of −80 mV, and an initial step at −40 mV was applied to inactivate Na^+ and T-type Ca^{2+} currents (Fig. S2 A). Peak I_{Ca} was subsequently measured at different membrane potentials (from −40 to 0 or −25 to 0 mV) at control and after 3 minutes of Iso application. The extent of SR Ca^{2+} loading was controlled and kept comparable, despite Iso application, with a train encompassing an appropriate number of depolarization steps (10 for control and 2 in the presence of Iso) of 200-ms duration at 0.5 Hz (Fig. S2 B). The train of depolarizations was preceded by a rapid caffeine exposure to initiate controlled SR Ca^{2+} loading from an empty SR. In further experiments, a different protocol was applied to ensure comparable I_{Ca} trigger strength, and comparable SR Ca^{2+} load between all groups (WT and S2030A$^{+/+}$ cells in both conditions, control and during Iso stimulation). After the same preconditioning protocol shown in Fig. S2 A, various sized currents were recorded (Fig. S2 C): from −40 to −25 up to 0 mV (+5-mV steps) in the control and from −40 to −35 up to −10 mV for Iso. With Iso, an extra recording was performed with a different range of I_{Ca} trigger (from −40 to −30 up to −15 mV, with +3-mV steps). Between the recorded currents, a matching pair was selected for each cell (WT and mutant), with the mean WT I_{Ca} used as a reference (±15%). A cell was included in the analysis when the difference between the I_{Ca} in control and Iso was within ±15%. The cells were finally selected according to their SR Ca^{2+} content (mean WT, ±15%). The cells that did not meet the criteria were excluded.

Confocal Ca^{2+} imaging and analysis

Ca^{2+} transients elicited by I_{Ca} at different test potentials were recorded by using the Ca^{2+}-sensitive fluorescent indicator fluo-3 pentapotassium salt (Biotium) dialyzed through the recording pipette. Changes in intracellular Ca^{2+} concentration ($[Ca^{2+}]_i$) were recorded with a confocal microscope (FluoView 1000, ×60 water immersion objective; Olympus) in the line-scan mode at a rate of ∼500 lines/s. Fluo-3 was exited at 473 nm with a solid-state laser (MLL-FN-473; Changchun New Industries Optoelectronics Technology Co.), and light emission was acquired at a wavelength of >500 nm. Line-scan images were analyzed with ImageJ software (National Institutes of Health) and IgorPro cus-

tom-written macros. Ca^{2+} sparks were quantified with the ImageJ plug-in "SparkMaster" (Picht et al., 2007).

Intact cardiomyocytes were loaded with 5 µmol/liter fluo-3 acetoxymethyl ester (AM) for 30 min at room temperature. After washout, 30 min were allowed for de-esterification. Laminin (10 µg/ml) was used to coat the coverslips and to minimize motion artifacts. To determine Ca^{2+} wave parameters, we elicited waves by elevating $[Ca^{2+}]_o$ to 10 mmol/liter, which resulted in SR Ca^{2+} overload and repetitive Ca^{2+} waves (Ullrich et al., 2012). A 20-s line-scan image was recorded before and 3 min after Iso application, and waves were analyzed for propagation velocity. After digital deskewing of the wavefront, the line profile of the Ca^{2+} wave was further analyzed for amplitude of the Ca^{2+} release and tau decay (τ) of the waves (Fig. S9 A). Spontaneous Ca^{2+} sparks, the Ca^{2+} wave frequency, and the latency of the first spontaneous Ca^{2+} wave were recorded after a train of electrical field stimulations at 1 Hz for 30 s (0.5-ms pulses at 20–40 V).

Spark recovery analysis

Isolated ventricular myocytes were loaded with fluo-3 AM (as described above) and with EGTA-AM (5 µmol/liter for 30 min, to suppress intracellular Ca^{2+} waves). Repetitive Ca^{2+} sparks originating from the same cluster of RyR2s were elicited with a very low ryanodine concentration (50 nmol/liter), as previously described (Ramay et al., 2011). Please note that, at such concentrations, presumably only a few RyRs have bound ryanodine and that all other channels within the active couplon remain in their native state. Only prolonged exposure to ryanodine will significantly increase the appearance of long-lasting Ca^{2+} release events. For this reason, for each cell, the data acquisition was limited to a few minutes (maximum, 8 min) until long-lasting release events started to appear. Active Ca^{2+} spark sites were identified and recorded by confocal microscopy in line-scan mode in control conditions and in the presence of 100 nmol/liter Iso. To reach steady-state, Iso was applied 3 min before recording. Analysis of repetitive Ca^{2+} sparks was performed with a custom program written in MatLab (MathWorks). The criteria of event selection were used as previously described (Ramay et al., 2011). In brief, myocytes with Ca^{2+} spark frequencies higher than 15 sparks/100 µm/s or cells with long-lasting sparks (>200 ms) were excluded from analysis. In addition, clusters with 2 subpopulations of events (in terms of amplitudes of releases) were excluded from the analysis, because they could reflect the overlap of two closely spaced clusters of RyR2. All spark-to-spark delays were included in the histograms. Amplitude ratios where the initial spark in the pair occurred within 200 ms of a previous event were excluded to ensure that the first spark in the pair occurred with a fully Ca^{2+}-loaded SR. Spark amplitude ratios were fitted with a single exponential curve.

Western blot analysis

Freshly isolated cardiomyocytes were treated with Iso at 100 nmol/liter, in experimental conditions similar to those used for the Ca^{2+} measurements. For a few experiments, a high dose of Iso (1 µmol/liter) was combined with the phosphatase inhibitors okadaic acid (OA; 10 µmol/liter, CAS no. 155716–06-6; Alomone Laboratories) to obtain maximal phosphorylation levels. For the control, an equal number of cells was treated with the vehicle. After treatment, the cells were lysed with the NP-40 Lysis Buffer kit (ref. FNN0021; Thermo Fisher Scientific) composed of (in mmol/liter) 150 NaCl, 1% NP-40, and 50 Tris Base (pH 8). The buffer was supplemented with anti-proteases (Complete Mini, ref. 4693124001; Roche) and anti-phosphatase cocktails (PhosSTOP, ref. 4906845001; Roche). Proteins were quantified with the Pierce BCA protein assay kit (no. 23227; Thermo Fisher Scientific). After quantification, 35–50 µg proteins was suspended with 4× Laemmli sample buffer freshly supplemented with 2-mercaptoethanol (10% vol/vol), and ultrapure water was used to adjust the final volume (40 µl). The proteins were separated by a 4–20% SDS-PAGE gradient gel (Mini-Protean TGX Stain-Free Gels, 60 min at 200 V; Bio-Rad) and transferred to a polyvinyldine difluoride membrane (0.45-µm pore size; BioRad) preactivated with pure ethanol (20 V for 16–18 h at 4°C). The membranes were subsequently blocked for 1 h at room temperature in PBS (ref. A 0975.9010; AxonLab) plus 3% BSA. Membranes were then incubated for 3 h in PBS-10% Tween with antibodies anti-phospho-RyR2-S2808 (1:2,000, A010-30AP, Badrilla), anti-phospho-RyR2-S2814 (1:500, A010-31AP; Badrilla), anti-dephospho-RyR2-S2030 (1:1,000), anti-RyR (1:1,000, C3-33, Ab2827; Abcam), and anti-glyceraldehyde phosphate dehydrogenase (GAPDH; 1:100,000, 10R-G109A; Fitzgerald Biosciences). After incubation with primary antibodies, the membranes were washed three times for 10 min in PBS-T-0.3% BSA. Membranes were then incubated with secondary anti-mouse and anti-rabbit antibodies conjugated to horseradish peroxidase (1:10,000, 115–035-146 and 111–035-144; Jackson ImmunoResearch). After washing three times for 10 min (PBS-Tween), protein–antibody reactions were detected with Western ECL Substrate (Clarity and Clarity Max, 1705060 and 1705062; Bio-Rad) and the ChemiDoc MP Imaging System (Bio-Rad). For some experiments anti-rabbit Alexa Fluor 680 and anti-mouse Alexa Fluor 790 were used as secondary antibodies (1:100,000). Densities of protein were measured with Image Lab Software (Life Science Research, Bio-Rad). The level of the phosphorylation was expressed as the ratio of RyR phospho-signal for each antibody and the total anti-RyR antibody signal, both normalized for the GAPDH signal used as the loading control.

Statistical analysis

Box-and-whisker plots and scatterplots were used in the figures to show the distribution of the dataset. Each point represents a single measurement from an individual cell. The whiskers cover the range from 10% to 90%. In the supplemental tables, data are expressed as means ± SEM of *n* measurements. The statistical analysis was performed with IgorPro software and IBM SPSS statistical software. The Shapiro-Wilk test was used to test the normal distribution. A logarithmic transformation was performed to improve the symmetry when the null hypothesis of the normality test was rejected. For the analysis, we used the hierarchical statistical methodologies as previously shown in Sikkel et al. (2017), with the number of animals (*N*) and the number of cells (*n*), followed by least-significant-difference multicomparisons (all performed in SPSS). Data were paired (experiments with one control and one or two test recordings per cell) unless otherwise indi-

cated. The nonparametric Kruskal-Wallis test was used to compare densities in Western blot experiments. Fisher's exact test was used to compare occurrence of Ca^{2+} waves between different groups. A bootstrap approach (Poláková et al., 2015) was used to compute 95% confidence intervals (CIs) for the spark-to-spark delay medians. $P < 0.05$ indicated statistically significant results.

Online supplemental material

Fig. S1 shows the comparison between the HW/BW ratios in WT and S2030A$^{+/+}$ mutant animals. Fig. S2 describes the recording protocols used for the electrophysiological measurements. Fig. S3 shows Western blots in which the anti-dephospho-S2030 Ab was tested on S2030A$^{+/+}$ protein extraction. Fig. S4 highlights the effect of Iso stimulation on PLB for WT and both S2030A$^{+/+}$ and S2808A$^{+/+}$ mutant myocytes. Fig. S5 indicates the consequences of cell permeabilization on RyR2 phosphorylation levels. Figs. S6 and S7 show the effects of combining 2D12 Fab and cAMP on Ca^{2+} wave frequency, on τ decay of the Ca^{2+} release, and on SR Ca^{2+} content. Fig. S8 shows the spark amplitude restitution used as the control of the successful β-adrenergic simulation in both WT and S2030A$^{+/+}$ during Iso treatment. Fig. S9 describes how the Ca^{2+} wave analysis was performed. Table S1 summarizes the cardiac functional characterization. Table S2 reports the statistical summary of the Ca^{2+} transient amplitude obtained from the ECC gain measurements under matched SR Ca^{2+} load and matched I_{Ca} density. Table S3 summarizes the Ca^{2+} sparks parameters.

Results

ECC gain is decreased in S2030A$^{+/+}$ myocytes after β-adrenergic stimulation at matched SR Ca^{2+} loading and matched I_{Ca}

The genetic ablation of the RyR2-S2030 site induces a mild structural remodeling of the heart. Comparing absolute echocardiographic measurements (Table S1), we found a slight but not significant increase in the left ventricular diastolic and systolic volume and a normal ejection fraction. Further, we found a higher HW-to-BW ratio in S2030A$^{+/+}$ mice (with no differences in BW), which may suggest cardiac hypertrophy (Fig. S1). However, the S2030A$^{+/+}$ line displays no overt phenotype. To compare ECC in WT and RyR2-S2030A$^{+/+}$ ventricular myocytes, we examined the functional coupling of LTCCs and RyR2. Specifically, we assessed the amount of Ca^{2+} released per unit of Ca^{2+} entry, defined as ECC gain (Ullrich et al., 2012). Applying the voltage–clamp protocols shown in Fig. S2, we simultaneously measured I_{Ca} and the triggered Ca^{2+} transients in control conditions (Fig. 1 A, black traces) and during application of Iso (red traces). Note that in Fig. 1 the SR Ca^{2+} content was experimentally standardized between control and Iso in all cells to minimize the influence of RyR2 modulation by SR luminal Ca^{2+} (Fig. S2 B; Ogrodnik and Niggli, 2010). The density of the currents and the amplitude of the Ca^{2+} transients were larger in mutant cardiomyocytes (Table 1). SR Ca^{2+} content was also significantly higher in mutant cells. Because of the different SR Ca^{2+} load between WT and S2030A$^{+/+}$ cells, the ECC gain was normalized to the amplitude of the caffeine-dependent Ca^{2+} transient. The ECC gain in the mutant myocytes was not different at low-triggering I_{Ca} (−25-mV step) compared with WT (Fig. 1 B), but it was significantly lower at the peak of the I_{Ca} (0 mV; Fig. 1 C). It has already been reported that β-adrenergic stimulation increases the current amplitude more than the Ca^{2+} transient (Bers, 2002). This finding, together with the experimentally matched SR Ca^{2+} load, explains the decrease in ECC gain during Iso stimulation for both animals (Fig. 1, B and C). Upon Iso application, the Ca^{2+} release is systematically enhanced with increasing load and/or increasing trigger (Ginsburg and Bers, 2004). Because of the differences in the ECC machinery reported, we also measured the ECC gain in conditions of matched SR Ca^{2+} load and matched I_{Ca} between all the groups (see Materials and methods and Fig. S2 for details). In these experimental conditions, a change in the gain more reliably reflects a change in RyR activity, because the other parameters are experimentally controlled. In brief, the cells were selected according to their SR Ca^{2+} content, and the I_{Ca} trigger was maintained constant between groups with a recording protocol with variably sized I_{Ca} (see Fig. S2 C) and by selecting matching pairs of recordings. As previously shown (Ginsburg and Bers, 2004), in these experimental conditions, the ECC gain in WT myocytes was not significantly affected by Iso (Fig. 1 D). However, the ECC gain was decreased in S2030A$^{+/+}$ cells after Iso application, mostly because of a reduced Ca^{2+} release during β-adrenergic stimulation (Table S2). These results suggest that ablation of the RyR2-S2030 site affects Ca^{2+} release during Iso stimulation and hint at the functional importance of S2030 phosphorylation during β-AR activation.

Iso application increases RyR2-S2030 phosphorylation in WT myocytes

To verify Iso-dependent phosphorylation of the RyR2-S2030 site, we performed Western blot experiments. Cell homogenates were prepared from freshly isolated myocytes in similar experimental conditions as for Ca^{2+} measurements. We first measured the RyR2 protein expression level by using an anti-RyR Ab, and we found that the mutation decreased RyR expression level by ∼43% in S2030A$^{+/+}$ cells (Fig. 2 A). Then, we assessed the RyR2-S2030 phosphorylation state in WT myocytes before and after treatment with Iso using an Ab against dephospho-RyR2-S2030, which specifically detects the unphosphorylated state of the RyR2-S2030 site. We found that Iso application significantly decreased the fraction of dephospho-RyR2-S2030/RyR in WT ventricular myocytes, consistent with an increase of the S2030 phosphorylation (Fig. 2 B). In S2030A$^{+/+}$ protein extractions, the anti-dephospho-Ab also revealed a band, but the intensity of this signal was substantially lower compared with WT and, importantly, did not change upon Iso application (Fig. S3). The reduction of the dephosphorylation level generated by Iso treatment in WT cells provided evidence of an increase in S2030 phosphorylation during our experimental conditions. To obtain the maximal level of RyR2-S2030 phosphorylation, we treated cells with a high dose of Iso (1 µmol/liter) in combination with the phosphatase inhibitor okadaic acid (OA; 10 µmol/liter). Together, high Iso and OA further decreased the fraction of dephospho-RyR2-S2030/RyR compared with Iso alone (100 nmol/liter; Fig. 2 C). Considering this level as the 100% phosphorylation state of the RyR2-S2030, the Iso concentration used in our experiments (100 nmol/liter) resulted in an ∼55% phosphorylation of the site. Please note that

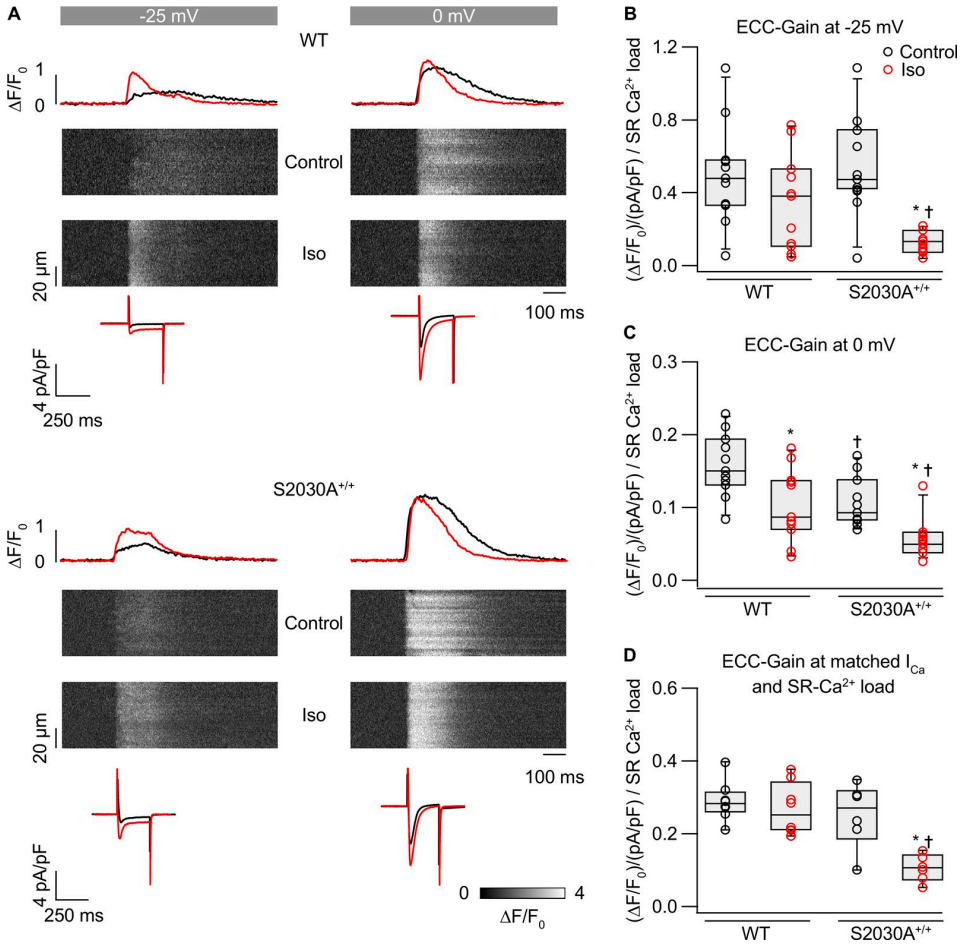

Figure 1. **ECC gain is decreased in S2030A$^{+/+}$ myocytes after β-adrenergic stimulation and matched SR Ca^{2+} loading. (A)** Depolarization of voltage-clamped cells from −40 to −25 mV (left) or to 0 mV (right) in control conditions and during β-adrenergic stimulation with 100 nmol/liter Iso (N = 5, *n* = 11 for both WT and S2030A$^{+/+}$ animals). The figure shows representative line profiles of the Ca^{2+} transients ($\Delta F/F_0$; black traces for control and red for Iso), confocal line-scan images, and I_{Ca} traces for both WT and S2030A$^{+/+}$ cells. **(B and C)** ECC gain was obtained from the ratio of the maximal Ca^{2+} transient amplitude and the peak I_{Ca} density $(\Delta F/F_0)/(pA/pF)$, normalized to the SR Ca^{2+} content. **(D)** The ECC gain was obtained in conditions of matched SR Ca^{2+} load and I_{Ca} between all cell groups. The gain was minimally influenced by Iso in WT cells. However, the mutation affected the ECC gain ratio in Iso, mostly because of a decreased Ca^{2+} release during β-adrenergic stimulation (see Table S2). Please note that in this experiment, the SR Ca^{2+} content was experimentally matched between control and Iso. *, P < 0.05, Iso versus control; †, P < 0.05, S2030A versus WT. The whiskers cover the range from 10% to 90%.

the decreased expression of RyRs observed in S2030A$^{+/+}$ mice is not expected to substantially affect Ca^{2+} spark properties, unless the number of RyRs per couplon becomes very low (Sobie et al., 2002).

Ablation of the S2030 site prevents the increase of the CaSpF upon β-adrenergic stimulation during rest

To further test the hypothesis that S2030 may represent a mechanistically relevant link between β-adrenergic stimulation and RyR2 modulation, we explored the consequences of the S2030 site ablation on the resting spontaneous Ca^{2+} release. We compared Ca^{2+} spark frequency (CaSpF) between WT and S2030A$^{+/+}$ myocytes in control and during Iso application (Fig. 3). In view of recent studies in several laboratories demonstrating that CaSpF increases rapidly in quiescent cells during β-adrenergic stimulation (Gutierrez et al., 2013; Dries et al., 2016), a modified responsiveness of the mutant RyR2-S2030A$^{+/+}$ receptors may result in a lower CaSpF in Iso. In intact cells loaded with fluo-3, basal CaSpF was similar between WT and S2030A$^{+/+}$ cardiomyocytes (Fig. 3 B; mean CaSpFs are reported in Table S3; for median values, see boxplots in the figures). After application of Iso, the frequency of sparks became two times higher in WT compared with S2030A$^{+/+}$ cells. As a positive control, we performed the same experiment in another mouse model with a mutation at the RyR2-S2808 site, the second PKA-dependent phosphorylation site identified on RyR2. In Iso, CaSpF was significantly higher in S2808A$^{+/+}$ cardiomyocytes than S2030A$^{+/+}$ cardiomyocytes (Fig. 3 B), confirming the potentially important role of the S2030 site during the β-adrenergic response. Interestingly, Iso treatment did not increase spark amplitudes and the related spark mass in S2030A$^{+/+}$ cells (Table S3). These results confirm the blunted response of the S2030A$^{+/+}$ mutant myocytes to Iso and suggest that S2030

Table 1. **Statistical summary of the I_{Ca} density and the Ca^{2+} transient amplitude**

	I_{Ca} density	I_{Ca} density	Transient amplitude	Transient amplitude	SR Ca^{2+} content
	−40/−25 mV (pA/pF)	**−40/0 mV (pA/pF)**	**−40/−25 mV ($\Delta F/F_0$)**	**−40/0 mV ($\Delta F/F_0$)**	**($\Delta F/F_0$)**
WT (N = 5/*n* = 11)					
Control	0.44 ± 0.16	4.83 ± 0.43	0.45 ± 0.09	2.23 ± 0.29	2.84 ± 0.29
Iso	1.98 ± 0.61[a]	8.73 ± 0.95[a]	1.09 ± 0.23[a]	2.47 ± 0.36[a]	2.96 ± 0.35
S2030A (N = 5/*n* = 11)					
Control	0.89 ± 0.39	6.87 ± 0.43[b]	1.04 ± 0.13[b]	2.93 ± 0.16[b]	4.46 ± 0.25[b]
Iso	2.93 ± 0.93[a]	10.82 ± 1.23[a]	1.01 ±0.14	2.3 ± 0.19	4.51 ± 0.24

I_{Ca} and transients were measured in freshly isolated ventricular cardiomyocytes of WT and S2030A$^{+/+}$ knock-in mice. Peak I_{Ca} was recorded at different membrane potentials (from −40 to 0 mV or −25 to 0 mV) in control conditions (1.8 mM $[Ca^{2+}]_o$) and during 100 nmol/liter Iso application. The protocol shown in Fig. S2 was used to experimentally match the SR Ca^{2+} content between control and Iso in all cells. At matched SR Ca^{2+} load, the Ca^{2+} release in S2030A$^{+/+}$ myocytes did not increase during Iso, suggesting a decreased RyRs sensitivity (see Fig. 1). Data are expressed as means ± SEM of *n* measurements.
[a]P < 0.05 versus control.
[b]P < 0.05 versus WT.

site ablation interferes with RyR2 sensitization upon β-adrenergic stimulation. Discrepancies in CaSpF between WT and RyR2-S2030A$^{+/+}$ animals could not be explained by different SR Ca^{2+} loading (which was similar between groups; Fig. 3 C) or by the SERCA pump stimulation (measured as τ decay of the global Ca^{2+} transient), which was not significantly different between animals (Fig. S4). Unlike in the previous experiment, the SR Ca^{2+} load was not matched between control and Iso, and SERCA acceleration resulted in a slightly increased SR Ca^{2+} content. Higher SR Ca^{2+} load in turn may partly contribute to the elevated CaSpF in Iso in both WT and S2030A$^{+/+}$ cells. Therefore, we conceived a series of experiments in permeabilized cardiomyocytes, with the strategy being to remove SERCA stimulation by cAMP (and thus changes in intra-SR Ca^{2+}) as a variable.

cAMP increases CaSpF and SR Ca^{2+} load in WT and S2030A$^{+/+}$ myocytes

Iso can stimulate phosphorylation of RyR2 as well as phospholamban (PLB) and LTCC, thereby increasing Ca^{2+} release from the SR, SR Ca^{2+} content, and Ca^{2+} entry. Because of these substantial changes in ECC, it was challenging to dissect the precise functional consequences of RyR2 phosphorylation during β-adrenergic stimulation. To remove most of these variables and confirm a direct modulation of RyR2 in its cellular environment, we investigated spontaneous Ca^{2+} release events in permeabilized myocytes. Free $[Ca^{2+}]$ was clamped at 50 nmol/liter, and cAMP was used to activate PKA. In these experiments, basal CaSpF was again similar between WT and S2030A$^{+/+}$ cardiomyocytes (Fig. 4 B i), suggesting no functional differences in control conditions. Spark frequency was increased by cAMP to similar levels in both WT and S2030A$^{+/+}$ myocytes, reaching the peak after 5–7 min (Fig. 4 B i). This finding initially seemed to be in disagreement with our observations made earlier in intact cells (see Fig. 3). Because it has recently been reported that membrane permeabilization by itself may provoke a progressive increase in the RyR2 phosphorylation level at the S2808 site (Bovo et al., 2017), we examined whether this phenomenon was occurring in our conditions and was the reason for the discrepancy. Using a phosphospecific Ab, we did not detect differences in the phosphorylation level at the S2808 site before and after 20 min of permeabilization (Fig. S5). We also observed that the cAMP-dependent increase in CaSpF was associated with an elevated SR Ca^{2+} content in both cell types (Fig. 4 B ii). Because RyR2 activity highly depends on the SR luminal $[Ca^{2+}]$, the lack of differences between WT and S2030A$^{+/+}$ myocytes may be partially caused by the elevated SR Ca^{2+} loading. This effect may obscure differences in RyR2 activity between WT and S2030A$^{+/+}$ cells during cAMP stimulation.

cAMP does not increase CaSpF in S2030A$^{+/+}$ myocytes after maximal stimulation of the SERCA pump

To separate the direct consequences of RyR2 phosphorylation from the indirect effect via changes in SR Ca^{2+} content, we pretreated the permeabilized myocytes with the PLB monoclonal Ab (2D12) that has been shown to bind PLB and accelerate SERCA activity in permeabilized cells. To facilitate the penetration of 2D12 into the cytosol (Chan et al., 2015), we digested the antibody and purified only the Fab. 2D12-Fab accelerated the τ decay of global Ca^{2+} signals, indicating a faster SERCA. The addition of cAMP did not further accelerate the pump, suggesting maximal stimulation by the Fab (Fig. S6). As a result of the elevated SR Ca^{2+} level, CaSpF was already increased in control conditions compared with basal frequency (Fig. 4 D). Starting from maximal SERCA stimulation, cAMP application further increased CaSpF in WT myocytes, but not in S2030A$^{+/+}$ cells (Fig. 4 D). The SR Ca^{2+} content was lower in these cells after treatment with cAMP (Fig. S7), most likely because of the larger RyR2-mediated Ca^{2+} leak in WT myocytes. These observations suggest that, when SERCA activity is kept constant (see Fig. S6), the addition of cAMP unmasks an insensitivity of RyR2-S2030A$^{+/+}$ channel activity toward PKA-dependent phosphorylation, similar to and consistent with the observations in intact cells shown in Fig. 3. These results confirm a direct modulation of RyR2 in the cellular environment and lend additional support to the notion that the S2030 site plays an important role in RyR2 modulation during the β-adrenergic response.

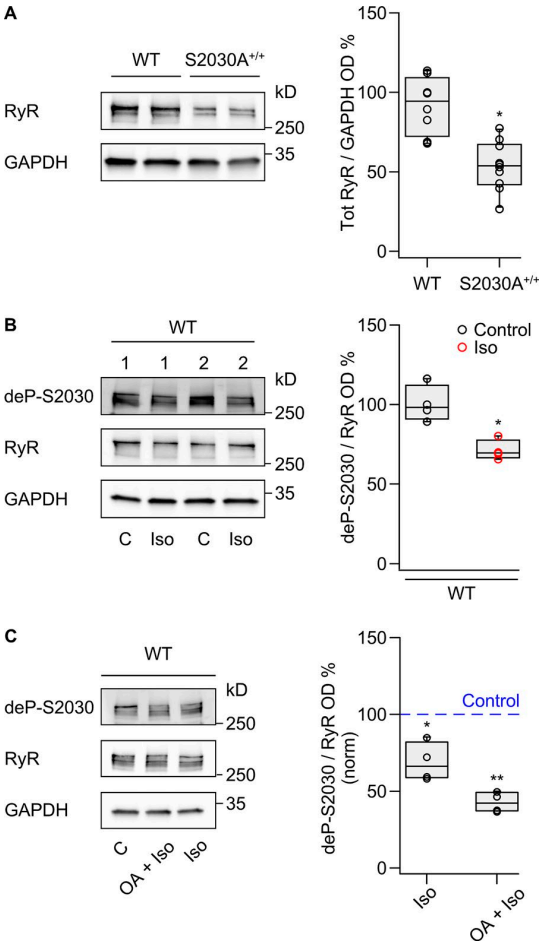

Figure 2. **RyR2-S2030 site phosphorylation level is increased by Iso stimulation. (A)** Representative blot showing total RyR2 expression levels in WT (N = 8) and S2030A$^{+/+}$ (N = 10) animals. **(B)** Representative blot showing the level of dephosphorylation at RyR2-S2030 site in WT animals (N = 4), before (C, control) and after 100 nmol/liter Iso application. The numbers 1 and 2 identify different animals. The level of the phosphorylation was expressed as the ratio of the dephospho-RyR2-S2030 and the total RyR ODs, both normalized for the GAPDH signal. Please note that a low level of dephosphorylation corresponds to a high level of phosphorylation. **(C)** Representative blot showing the maximal level of dephosphorylation at the RyR2-S2030 site in WT animals (N = 4) obtained with a high dose of Iso (1 µmol/liter) combined with the phosphatase inhibitor OA (10 µmol/liter). The dephosphorylation levels were normalized to the control (100%). Iso at the concentration used in all experiments (100 nmol/liter) resulted in a decrease in the signal corresponding to an increased level of phosphorylation (69 ± 6% compared with the control). The combination of high Iso concentration and OA further decreased the signal (44.4 ± 4%). The data are expressed as mean ± SEM of all measurements. *, P < 0.05 versus control; **, P < 0.05, Iso versus OA + Iso.

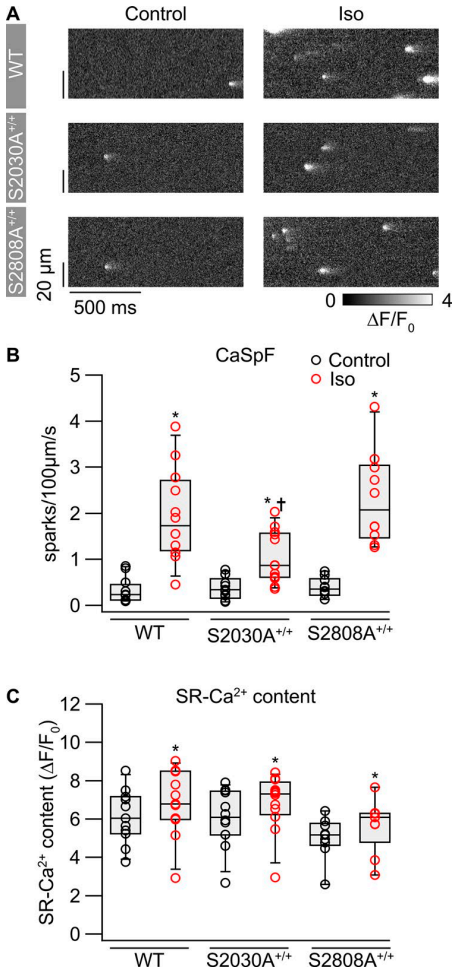

Figure 3. **S2030 site ablation limits the Iso-dependent increase in CaSpF. (A)** Confocal line-scan images showing Ca^{2+} sparks in intact cells in control and after 3 min of 100 nmol/liter Iso treatment for WT (N = 4, *n* = 12), S2030A$^{+/+}$ (N = 4, *n* = 13), and S2808A$^{+/+}$ (N = 3, *n* = 10) myocytes. **(B)** The basal CaSpF (number of sparks per 100 µm/s) was similar among the animal groups; after application of Iso, the CaSpF in S2030A$^{+/+}$ myocytes was significantly lower compared with WT and S2808A$^{+/+}$ cells. **(C)** SR Ca^{2+} content was not significantly different between the mouse models. Please note that unlike in the patch-clamp experiments, the SR Ca^{2+} load here was not matched between control and Iso. *, P < 0.05 versus control; †, P < 0.05 versus WT. The whiskers cover the range from 10% to 90%.

The S2030 site is involved in Ca^{2+} spark-to-spark delay shortening during β-adrenergic stimulation

The rate of recovery of Ca^{2+} sparks after termination (i.e., the temporal distribution of their refiring probability) can be used as a tool to assess the Ca^{2+} sensitivity of the RyRs in situ. Interventions that are thought to sensitize RyRs (e.g., Iso and caffeine) or inhibit the channels (e.g., tetracaine) can actively shorten or prolong the spark-to-spark delay time, respectively (Poláková et al., 2015). According to our previous results, we hypothesized that Ca^{2+} spark recovery time would be shortened to a lesser extent by Iso in S2030A$^{+/+}$ myocytes. To investigate this hypothesis, we performed a Ca^{2+} spark recovery analysis by using the method illustrated in Fig. 5 A (Sobie et al., 2005). In this method, a low dose of ryanodine was used to increase the frequency of Ca^{2+} sparks. The ryanodine-bound RyRs act as Ca^{2+} source and drive the repetitive firing of RyR2 clusters (1–10 per cell) for a limited period of time (see Fig. 5 A and paragraph "Relation to previous work and limitations" of the Discussion; Sobie et al., 2005). Taking advantage of this feature of the RyR–ryanodine binding, we perfused the isolated myocytes with ryanodine at a concentration of 50 nmol/liter (see Materials and methods for details). After the

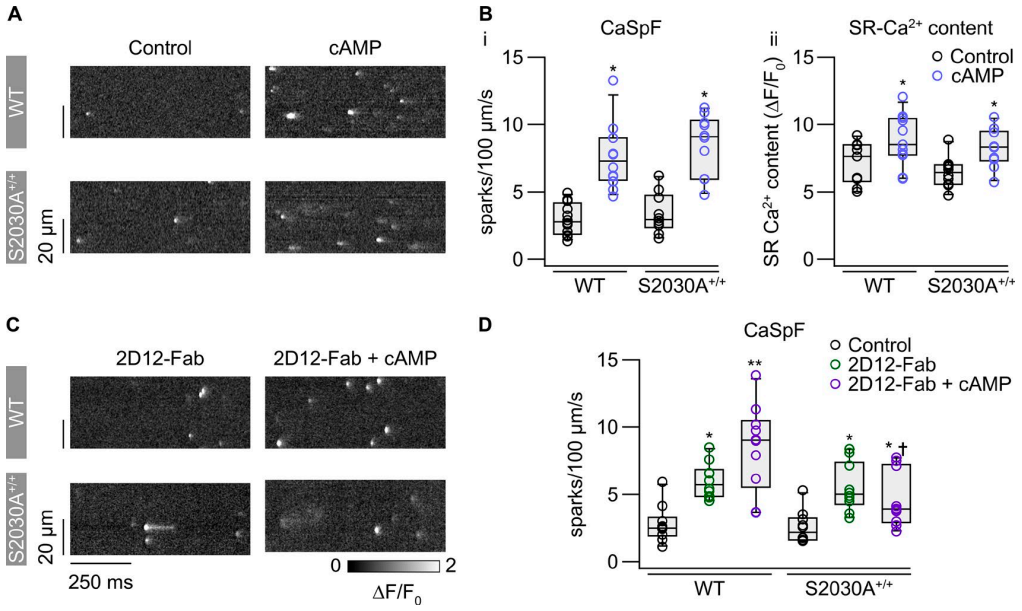

Figure 4. **Maximal SERCA stimulation unmasks a limited cAMP-dependent increase in CaSpF. (A)** Representative confocal line-scan images showing Ca^{2+} sparks in β-escin permeabilized cells before and after 5 min in 5 µmol/liter cAMP. **(B)** Basal CaSpF was similar for WT (N = 5, *n* = 12) and S2030A$^{+/+}$ (N = 4, *n* = 10; 2.98 ± 0.34 vs. 3.39 ± 0.47 sparks per 100 µm/s, respectively; i). cAMP enhanced SpF in both cell types. SR Ca^{2+} content was increased after treatment with cAMP (ii). **(C)** Confocal line-scan images showing Ca^{2+} sparks in myocytes pretreated with 100 µg/ml 2D12-Fab (15 min) before and after cAMP application. **(D)** 2D12-Fab increased basal CaSpF (6.01 ± 0.41 vs. 5.51 ± 0.56 sparks per 100 µm/s, respectively) for WT (N = 6, *n* = 10) and S2030A$^{+/+}$cells (N = 4, *n* = 10); cAMP further increased CaSpF only in WT cells. *, P < 0.05 versus control; **, P < 0.05 versus 2D12-Fab; †, P < 0.05 versus WT. The whiskers cover the range from 10% to 90%.

recordings, we analyzed the spark-to-spark delay for each Ca^{2+} spark pair (Fig. 5) and the recovery time course of the Ca^{2+} spark amplitude (Fig. S8; see Materials and methods for the criteria of event selection). Specifically, the median of the spark-to-spark delays histogram was adopted as a parameter defining RyR2s Ca^{2+} sensitivity and the spark amplitude recovery time to estimate the local refilling of the SR. In control conditions, medians were not significantly different between WT and mutant cells (Fig. 5, B i and B iii), suggesting no major differences in basal RyR2 sensitivity. Iso application left shifted the median of the spark-to-spark delay histogram (i.e., shortened the interval) in WT myocytes, implying an increase in RyRs Ca^{2+} responsiveness (Fig. 5 B ii). As opposed to WT cells, S2030A$^{+/+}$ cells did not respond to Iso, and there was no shift of the median value (Fig. 5 B iv). The recovery of the spark amplitude was accelerated by Iso in both WT and S2030A$^{+/+}$ cells, confirming successful β-adrenergic simulation (Fig. S8). These results confirm that phosphorylation at the S2030 site may account for the increased RyR2 sensitivity during the β-adrenergic response in WT cardiomyocytes.

Ablation of the S2030 site decreases propensity for spontaneous whole-cell Ca^{2+} release

In cardiac myocytes, a Ca^{2+} wave is a global Ca^{2+} signal that spreads along the cell and is driven by CICR. During each wave, an excess of Ca^{2+} in the cytosol is extruded by the electrogenic Na^+–Ca^{2+} exchanger that can generate a DAD, which could trigger an action potential in a single cell (Willis et al., 2016). Changes in RyR2 function may alter the propensity for spontaneous Ca^{2+} waves (SCaWs) in S2030A$^{+/+}$ cardiomyocytes. To test this hypothesis, we measured the occurrence of waves and the latency to the first SCaW after a train of stimulations, an indicator of arrhythmogenicity at the single-cell level (Fig. 6). In control conditions, we observed a similar rate of occurrence of SCaW (percentage of cells showing Ca^{2+} waves) between WT and mutant cells (Fig. 6 C). Iso markedly elevated SCaW occurrences in WT myocytes, but we found an only moderate response to β-adrenergic stimulation in the mutant cells. Similarly, Iso significantly shortened the mean latency to the first SCaW in WT myocytes, but not in S2030A$^{+/+}$ myocytes (Fig. 6 B). Thus, ablation of the S2030 site reduced the propensity for whole-cell Ca^{2+} waves in isolated cardiomyocytes.

The RyR2-S2030A$^{+/+}$ mutation may also affect the spreading of Ca^{2+} waves. Because the speed of Ca^{2+} wave propagation has been linked to RyR's Ca^{2+} sensitivity (Ullrich et al., 2012), we compared Ca^{2+} wave propagation between WT and mutant cardiomyocytes before and after application of Iso (Fig. 6 D). To evoke a high frequency of Ca^{2+} waves, we elevated the extracellular Ca^{2+} concentration to 10 mmol/liter, which resulted in SR Ca^{2+} overload (for the protocol used, see Fig. S9). In this condition, the SR Ca^{2+} content is closer to its maximal level, and a difference in wave speed more directly reflects a change in RyR sensitivity. In control conditions, there were no differences in wave speed between WT and S2030A$^{+/+}$ myocytes, but after application of Iso, only WT cells showed an acceleration of the Ca^{2+} wave (Fig. 6 D). The lack of wave speed acceleration again confirmed the blunted response of CICR in S2030A$^{+/+}$ cells upon β-AR stimulation. The frequency of waves was slightly increased by Iso in both cell

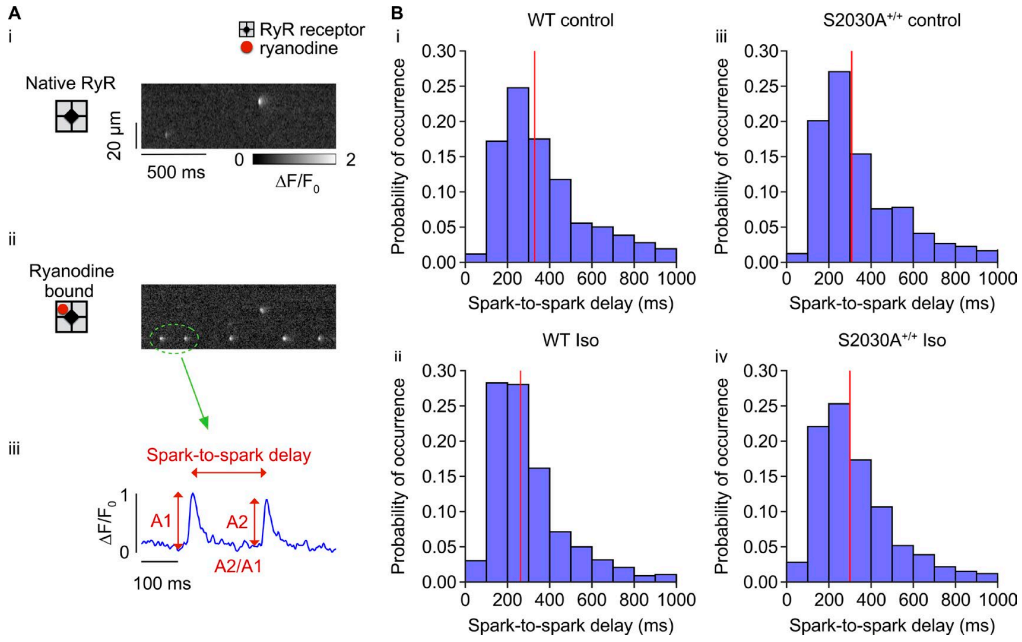

Figure 5. **Ca^{2+} spark-to-spark delay shortening is blunted during β-adrenergic stimulation in S2030A$^{+/+}$ cells. (A)** Representative line-scan image in control conditions (i). A very low concentration of ryanodine (50 nmol/liter) entrains repetitive sparks after binding to only a single monomeric RyR channel subunit in an entire couplon (ii). The spark-to-spark delay and the relative spark amplitudes were measured to investigate Ca^{2+} spark restitution (iii). **(B)** Histograms of spark-to-spark delays for control WT (328.8 ms, 95% CI, 313.8–348.3 ms; N = 10, *n* = 36, 937 spark pairs; i), Iso WT (261.8 ms, 95% CI, 254.5–269.4 ms; N = 11, *n* = 44, 1,783 spark pairs; ii), control S2030A$^{+/+}$ (308.3 ms, CI 95%: 291.6–329.2 ms; N = 6, *n* = 20, 488 spark pairs; iii), and Iso S2030A$^{+/+}$ cells (299.6 ms, CI 95%: 286.0–310.9 ms; N = 7, *n* = 27, 929 spark pairs; iv). Red lines identify the median values.

types. However, no significant differences were found between WT and S2030A$^{+/+}$ cells in control conditions (0.15 ± 0.02 and 0.19 ± 0.02 waves/s for WT and S2030A$^{+/+}$ cells, respectively) and after Iso treatment (0.29 ± 0.02 waves/s for WT cells and 0.37 ± 0.04 waves/s for S2030A$^{+/+}$ cells [mean ± SEM]).

RyR2-S2030A$^{+/+}$ mice show adaptive changes at RyR2-S2808 and S2814 phosphorylation sites

Using phosphospecific antibodies, we examined whether the RyR2 phosphorylation state at S2808 and S2814 could be altered as an indirect consequence of the mutation (Fig. 7 A). We observed a 1.8-fold increase in the phosphorylation level at RyR2-S2808 and a twofold increase in phosphorylation at RyR2-S2814 in mutant myocytes (Fig. 7, B and C). Presumably, the ablation of the S2030 site caused adaptive changes in RyR2 phosphorylation at the other two major phospho-sites. However, treatment with Iso elevated RyR2 phosphorylation at S2808 and S2814 in both WT and S2030A$^{+/+}$ cells (Fig. 7, B and C). These results confirmed that the basal phosphorylation at these two sites was not saturated in S2030A$^{+/+}$ myocytes and could be further increased by Iso stimulation. Therefore, the adaptive modifications of the other RyR2 phosphorylation levels cannot underlie the absence of functional RyR2s changes in S2030A$^{+/+}$ myocytes.

Discussion

During episodes of stress or exercise, activation of the β-adrenergic pathway enhances Ca^{2+} entry via LTCC and Ca^{2+} reuptake into SR store by SERCA stimulation. These mechanisms boost the beat-to-beat Ca^{2+} release, eventually leading to a stronger myocardial contraction. Phosphorylation at specific RyR2 sites may enhance Ca^{2+} release during a β-adrenergic response, possibly contributing to positive inotropy and/or Ca^{2+}-induced arrhythmias. Recently, the RyR2-S2030 phosphorylation site has been identified and proposed as the major PKA target on RyR2 upon β-AR stimulation. The information available in the literature on S2030 is limited and largely based on in vitro assays. Therefore, to explore the functional role of the S2030 site in the native cellular environment, we engineered an RyR2-S2030A$^{+/+}$ knock-in mouse in which the serine can no longer be phosphorylated.

Modulation of RyR2 function during β-adrenergic response

The functional consequences of RyR2s phosphorylation have attracted much recent attention. The interest in the topic grew when PKA-dependent phosphorylation of RyR2 at S2808 was proposed as the major impairment that contributes to HF progression (Marx et al., 2000). However, S2808 was found to be already substantially phosphorylated at rest in several animal species (~50–75%), raising doubts about the reliability of this site as an index of the PKA phosphorylation state (Xiao et al., 2005; Huke and Bers, 2008; Fischer et al., 2013). In our work, we found a decreased propensity for spontaneous Ca^{2+} release in S2030A$^{+/+}$ cells (Figs. 3 and 6), which suggested an important role for the S2030 site in the modulation of RyR2. The blunted response to Iso cannot be explained by the higher SR Ca^{2+} load and larger I_{Ca} (Fig. 1), which would rather enhance the Ca^{2+} release propensity.

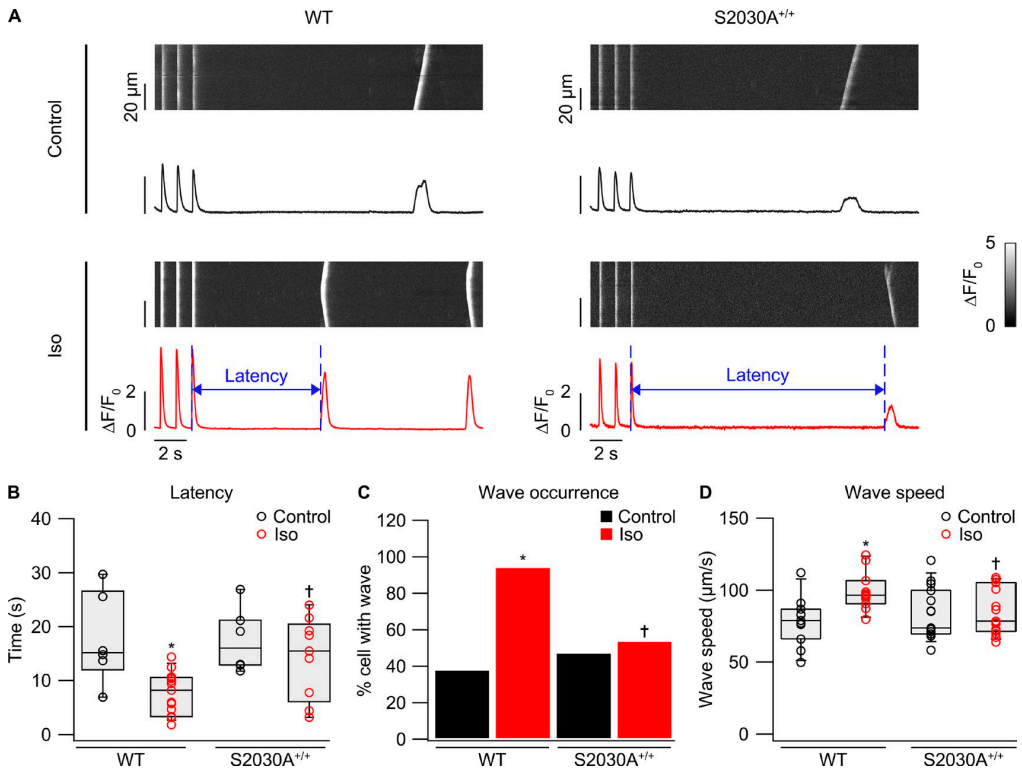

Figure 6. **Iso does not modify the latency of the first spontaneous Ca^{2+} release in S2030A$^{+/+}$ myocytes. (A)** Line-scan images were recorded in the end of a train of electrical stimulations at 1 Hz for 30 s. Each cell was recorded in control and after 3 min of 100 nmol/liter Iso treatment. The figure also shows line profiles of the triggered Ca^{2+} transients and the spontaneous Ca^{2+} releases ($\Delta F/F_0$; black traces for the control and red for Iso). The latency was calculated considering the last electrical stimulus and the first spontaneous Ca^{2+} release (arrows). **(B)** SCaW latency (17.72 ± 3.42 s vs. 8.08 ± 1.16 s), respectively, for control and after Iso stimulation for WT (18.04 ± 1.95 s for control vs. 14.27 ± 2.51 s for Iso in S2030A$^{+/+}$). Latency values were not paired, because not all cells displayed SCaW. **(C)** Occurrence of spontaneous release (percentage of cells that show at least one Ca^{2+} wave; N = 4, *n* = 16 for WT; N = 4, *n* = 15 for S2030A$^{+/+}$). **(D)** Comparison of wave speed (WT: N = 4, *n* = 11; 78.42 ± 5.05 µm/s [control] vs. 99.31 ± 4.03 µm/s [Iso]); S2030A$^{+/+}$: N = 4, *n* = 15; 83.49 ± 5.56 µm/s [control] vs. 85.40 ± 4.64 µm/s [Iso]). In all experiments shown, the SR Ca^{2+} load was not matched experimentally between control and Iso. *, P < 0.05 versus control; †, P < 0.05 versus WT. The whiskers cover the range from 10% to 90%.

Both alterations, as well as the RyR down-regulation (Fig. 2), are likely to be adaptive. Nevertheless, using a series of experimental approaches that minimize the variability of both, triggering Ca^{2+} and SR Ca^{2+} content (see Figs. 4 and 5), the S2030A$^{+/+}$ myocytes still exhibited a substantial insensitivity to PKA activation. The down-regulation of RyR2 could result from a lower number of couplons and/or a reduction of the number of RyRs per couplon. However, the number of couplons was found to be unchanged in S2030A$^{+/+}$ mice (Asghari et al., 2017). Furthermore, the down-regulation does not appear to compromise ECC in basal conditions (Fig. 1 B). Regarding a reduced number of channels per couplon, it is generally assumed that the expression of RyRs per couplon has a significant redundancy and does not limit the SR Ca^{2+} release, unless the number of channels per Ca^{2+} release site becomes very low (Sobie et al., 2002). Further, a small reduction in RyRs is not expected to affect spark parameters significantly (Cannell et al., 2013). Therefore, the decreased expression of total RyR presumably did not play a major role in our results.

In this work, we reported a higher baseline phosphorylation at the S2808 and S2814 in S2030A$^{+/+}$ animals, which most likely reflects adaptive modifications as a consequence of S2030 removal. As part of a compensatory change, the higher phosphorylation at these two sites may overall enhance the baseline Ca^{2+} release activity in the mutant cells. However, we did not detect major differences between WT and S2030A$^{+/+}$ cells in control conditions in terms of amount and kinetic of the spontaneous Ca^{2+} release (see Figs. 3, 4, and 6). Moreover, S2808 and S2814 phosphorylation levels were increased by Iso in S2030A$^{+/+}$ cells. These observations are consistent with the hypothesis that the S2030 site plays a role in the modulation of RyR2 activity. Our results also point out that the tentative RyR2 phosphorylation model developed so far may be too simplistic. A "multisite model" of RyR2 phosphorylation will most likely better define the RyR modulation (Valdivia, 2012; Camors and Valdivia, 2014). RyR2 regulation may depend on the combined effect of the kinases on a "phosphorylation hotspot" on the protruding side of the receptor (Yuchi et al., 2012) and other sites. S2030 is thought to be located in a region that may be involved in signal transduction between the transmembrane and cytoplasmic domains (Jones et al., 2008). Interestingly, in a previous study, we reported that the Ca^{2+} wave velocity was not increased by Iso in S2808A$^{+/+}$ myocytes, similar to what we now found for S2030A$^{+/+}$ cells (Ullrich et al., 2012). S2808 ablation

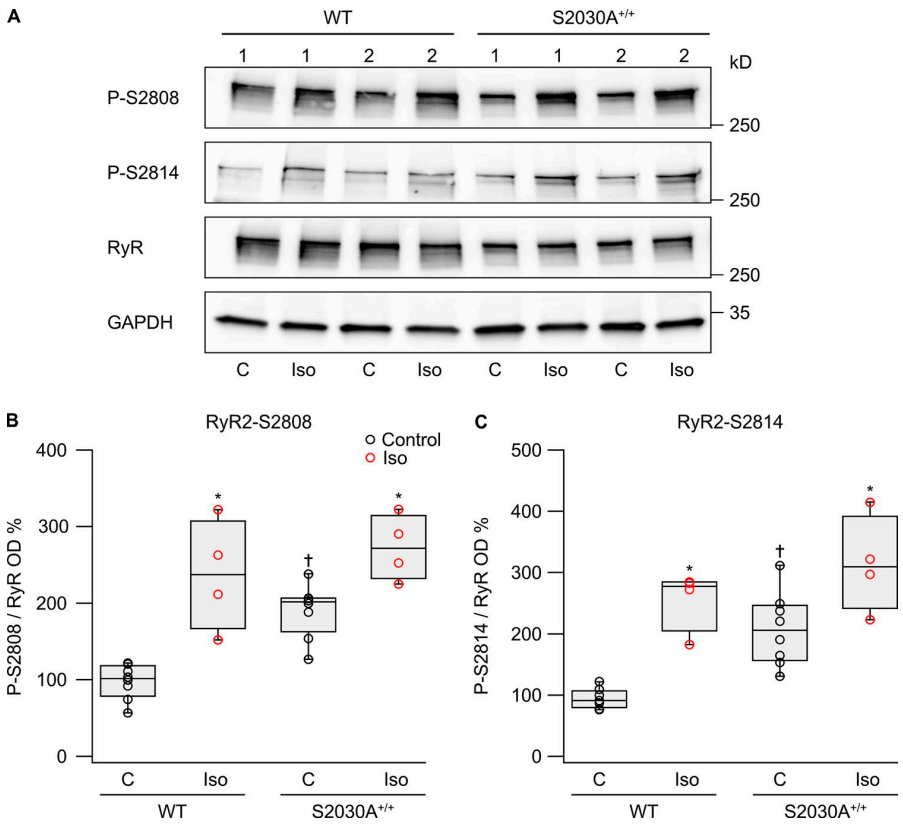

Figure 7. **S2030 ablation generates adaptive changes at RyR2-S2808 and S2814 phosphorylation sites in mutant cells. (A)** Representative blot showing the phosphorylation of RyR2 at the S2808 and S2814 sites in both WT and S2030A$^{+/+}$ cells in control (C) and during Iso stimulation. **(B and C)** The level of the phosphorylation was expressed as the ratio of the respective phospho- and total RyR ODs, both normalized to the GAPDH signal (N = 8 mice for both WT and S2030A$^{+/+}$ cells were used to compare baseline phosphorylation; between these, N = 4 animals were also assessed after Iso application). These data were tested for paired statistical difference. *, P < 0.05 versus control; †, P < 0.05 versus WT. The whiskers cover the range from 10% to 90%.

was also observed to prevent the decrease in spark-to-spark delays seen with β-adrenergic stimulation (Poláková et al., 2015). Despite the fact that consequences of S2808 phosphorylation are subtle and more difficult to detect, in terms of wave speed and spark-to-spark delay, the two animal models displayed similar behavior, which may suggest a functional link between the RyR2 regions harboring the mutations. Hence, our study shows that the S2030 site plays an important role in the modulation of RyR2 channels during the β-adrenergic response.

Role of RyR2 in pathophysiology

Excessive β-adrenergic stimulation may result in SR Ca^{2+} overload and increased diastolic SR Ca^{2+} release. In this study, we found that ablation of S2030 site reduces the cellular propensity for spontaneous Ca^{2+} release, suggesting that phosphorylation at the S2030 site is involved in changes in RyR2 sensitivity during β-adrenergic stimulation. The left shift in the spark-to-spark delay histogram, resulting from RyR2 sensitization was minimal and far smaller than the leftward shift observed in WT myocytes (Fig. 5). The longer refractoriness during β-adrenergic stimulation may desynchronize RyR2 cluster recruitment and partially explain the lack of wave speed acceleration we described. These data are consistent with previously published results showing that PKA does not increase the P_o of single RyR2 channels after ablation of the S2030 site (Xiao et al., 2007). This resistance toward β-adrenergic stimulation could also manifest itself in the probability for Ca^{2+} wave generation. We found a lower number of cells exhibiting spontaneous Ca^{2+} releases and no reduction of the first SCaW latency in S2030A$^{+/+}$ cells treated with Iso. These results show that ablation of the S2030 site decreases the spontaneous Ca^{2+} leak in isolated cells. Diastolic SR Ca^{2+} leak has been associated with HF, and gain- and loss-of-function mutations in RyR2 have been linked to CPVT (Marx et al., 2000; Ai et al., 2005; Xiao et al., 2005; Priori and Chen, 2011). Even though our work does not resolve the controversy over HF and CPVT development, the results suggest that preventing RyR2 phosphorylation at the S2030 site reduces the probability of initiating diastolic SR Ca^{2+} release and Ca^{2+} waves in isolated cardiomyocytes.

Potential therapeutic implications

Acute or chronic hyperadrenergic states can lead to the sensitization of the CICR mechanism that becomes unstable. β-AR blockers are widely used to reduce the risk for arrhythmias and sudden cardiac death. Several studies have been published suggesting that treatment with the Na^+ channel inhibitor flecainide or with β-blockers (e.g., carvedilol) could stabilize RyR2 function,

possibly via an off-target effect acting as RyR2 open-state blockers (Blayney and Lai, 2009; Hilliard et al., 2010). Unfortunately, β-AR blockers alone do not perfectly protect all patients in the long term. Therefore, additional strategies aimed at preventing arrhythmic events are clearly needed. Therapeutic approaches directed at stabilization of RyR2 are mechanistically attractive strategies. A novel class of RyR-stabilizing drugs, rycals, have been shown to improve contractile function in both heart and skeletal muscle (Andersson and Marks, 2010). However, many of the currently available RyRs stabilizers (e.g., JTV519) have off-target actions. Recently, dantrolene, a drug normally used to treat malignant hyperthermia, has also been shown to suppress arrhythmogenic SR Ca^{2+} release and DADs (Hartmann et al., 2017). Despite the promising outcomes of these studies, more work is needed to translate the studies of cells to the intact organism and to potential clinical applications. In this context of uncertainty, it is critical to identify novel compounds that could contribute to RyR2 and CICR stabilization. Our study suggests that the RyR2-S2030 site could be a new potential target to selectively reduce pathological SR Ca^{2+} leak without altering normal RyR2 and cardiac muscle function. The S2030A$^{+/+}$ transgenic mouse model is the first experimental system that specifically investigates the role of the RyR2-S2030 site in physiological conditions, and it is extremely difficult to translate our findings to different cellular systems. However, there is the possibility that the RyR2-S2030 site could actively participate in the RyRs modulation during the β-adrenergic response in human cardiac cells. If this were the case, then we speculate that this could represent a target for a specific reduction of a pathological SR Ca^{2+} leak in several conditions, such as CPVT and/or HF. More work is certainly required to extend these findings and explore this intriguing perspective.

Relation to previous work and limitations

With the intent to reveal a direct RyR2 modulation, we used the Fab of a PLB monoclonal antibody (2D12) to maximally accelerate SERCA activity, as previously shown (Chan et al., 2015). Starting from a fully stimulated SERCA, cAMP increased CaSpF in WT myocytes but not in S2030A$^{+/+}$ cells. These results confirmed that RyR2 can be directly modulated in the cellular environment and support the idea that the S2030 site plays an important role in RyR2 modulation. Our study seems to be at odds with results reported previously about the lack of a PKA effect on RyR2 in permeabilized cells devoid of PLB (Li et al., 2002). The discrepancy may come from different experimental conditions in terms of acute versus chronic removal of PLB-dependent modulation of SERCA. Moreover, our data do not exclude PKA-independent cellular mechanisms (e.g., Epac) that may play a role in RyR2 modulation at S2030 (Pereira et al., 2012). Nevertheless, we show that the S2030 site is important in RyR2 modulation regardless of the actual protein kinase activated by cAMP.

We measured the SR Ca^{2+} content using a similar approach in all experiments (assessing the peak of the caffeine-mediated transients). However, Figs. 1 and 3 show an apparent discrepancy regarding the difference in the SR Ca^{2+} load between WT and S2030A$^{+/+}$ cells. The higher baseline SR Ca^{2+} load in mutant cells reported in Fig. 1 is likely to arise from the larger Ca^{2+} entry in this condition (higher I_{Ca}; see Tables 1 and S2). The control over the Ca^{2+} entry is potentially less tight in electrical field stimulation (Fig. 3) than in patch-clamp experiments. When the cytosolic Ca^{2+} concentration was fixed in permeabilized cells (Fig. 4), we did not observe differences between WT and S2030A$^{+/+}$ cells in terms of SR Ca^{2+} content, suggesting that the amount of Ca^{2+} entry may be the reason of the discrepancy.

Recently, it has been reported that membrane permeabilization may progressively increase the RyR2 phosphorylation level at the S2808 site (Bovo et al., 2017). In our experimental conditions, 20 min of permeabilization did not modify the S2808 phosphorylation level. The divergence between the studies may lie in the permeabilization procedure itself. In our hands, β-escin seems to be a gentler agent for membrane permeabilization than saponin, and this may limit the loss of accessory proteins or factors adjusting phosphorylation.

In this study, we also analyzed the rate of recovery of Ca^{2+} sparks after termination, an indicator of the RyR Ca^{2+} sensitivity in situ (Fig. 5). In this approach, a low dose of ryanodine (50 nmol/liter) was used to increase the frequency of Ca^{2+} sparks (Sobie et al., 2005). Even though this approach provides information regarding the sensitivity of the RyRs in different experimental conditions (e.g., during caffeine or tetracaine treatment; Ramay et al., 2011), the use of ryanodine may have some limitations; it is not possible to determine the precise fraction of RyRs in the triggered cluster that act as Ca^{2+} source ("RyR drivers" with ryanodine bound), as well as the number of channels without ryanodine bound. Moreover, ryanodine may induce long-lasting RyR subconductance states and long Ca^{2+} sparks (Ramay et al., 2011). However, the ability of the cluster to refire is directly related to the sensitivity of the non–ryanodine-bound channels to react to the Ca^{2+} source. According to this idea, the repetitive nature of the recorded events (Fig. 5) suggests that at least some of the RyRs in the active site are in their native state. It is also important to consider that Ca^{2+} spark recovery was measured in resting cells, where most of the RyRs are in a closed state, and that ryanodine preferentially binds to open channels. Moreover, ryanodine was applied extracellularly, and its actual concentration may be substantially lower inside the cell during the first few minutes. All this may contribute to the small number of active sites (1–10 per cell) and the delayed appearance of the long-lasting events. In any case, to account for these potential problems, the data acquisition after ryanodine perfusion was limited to a maximum of 8 min or to the appearance of the first long-lasting Ca^{2+} release event (see Materials and methods for details and other exclusion criteria).

Conclusions

In summary, we present evidence at the cellular and near-molecular level of an important functional role for the S2030 phosphorylation site in RyR2 modulation during β-adrenergic stimulation. We show that ablation decreases the RyR2-mediated diastolic SR Ca^{2+} leak upon β-AR activation. In addition, we provide compelling evidence that interference with S2030 phosphorylation substantially reduces the cellular susceptibility for whole-cell Ca^{2+} release events, such as Ca^{2+} waves. Additional studies are needed to fully characterize the specific regulation of RyR2 at S2030 by PKA and other kinases in normal and diseased heart.

Acknowledgments

We thank Marianne Courtehoux and Michael Känzig for expert technical help, Stefan von Känel for software development, and Dr. Dmitry Terentyev for his gift of custom-made RyR antibodies.

This work was supported by the Swiss National Science Foundation (grant 310030-156375 to E. Niggli), the National Institutes of Health (grants HL055438, HL120108, and HL134328 to H.H. Valdivia), the Microscopy Imaging Center of the University of Bern (E. Niggli), the Graduate School for Cellular and Biomedical Sciences, University of Bern, and the Oetliker Foundation for Physiology (D.M. Potenza).

The authors declare no competing financial interests.

Author contributions: E. Niggli conceived and coordinated the study and designed the experiments. D.M. Potenza conducted the electrophysiological and fluorescence measurements on isolated intact and permeabilized ventricular cardiomyocytes, performed the related analysis, and wrote the manuscript, together with E. Niggli. D.M. Potenza and M. Fernandez-Tenorio performed the Western blot experiments. R. Janicek conducted the spark recovery experiments and carried out the associated analysis. H.H. Valdivia engineered and provided the S2030A$^{+/+}$ animal model. E. Camors and R. Ramos-Mondragón performed the echocardiographic recordings. All authors contributed to data analysis and interpretation as well as manuscript preparation.

Henk L. Granzier served as editor.

Submitted: 15 June 2018
Revised: 12 August 2018
Revised: 8 October 2018
Accepted: 22 October 2018

References

Ai, X., J.W. Curran, T.R. Shannon, D.M. Bers, and S.M. Pogwizd. 2005. Ca^{2+}/calmodulin-dependent protein kinase modulates cardiac ryanodine receptor phosphorylation and sarcoplasmic reticulum Ca^{2+} leak in heart failure. *Circ. Res.* 97:1314–1322. https://doi.org/10.1161/01.RES.0000194329.41863.89

Andersson, D.C., and A.R. Marks. 2010. Fixing ryanodine receptor Ca leak - a novel therapeutic strategy for contractile failure in heart and skeletal muscle. *Drug Discov. Today Dis. Mech.* 7:e151–e157. https://doi.org/10.1016/j.ddmec.2010.09.009

Asghari, P., D.R.L. Scriven, Y. Zhao, R. Ramos Mondragón, H. Valdivia, X. Wehrens, and E.D.W. Moore. 2017. RyR2 tetramer distributions in ventricular myocytes from phosphomutant mice. *Biophys. J.* 112:161a. https://doi.org/10.1016/j.bpj.2016.11.886

Benkusky, N.A., C.S. Weber, J.A. Scherman, E.F. Farrell, T.A. Hacker, M.C. John, P.A. Powers, and H.H. Valdivia. 2007. Intact beta-adrenergic response and unmodified progression toward heart failure in mice with genetic ablation of a major protein kinase A phosphorylation site in the cardiac ryanodine receptor. *Circ. Res.* 101:819–829. https://doi.org/10.1161/CIRCRESAHA.107.153007

Bers, D.M. 2002. Cardiac excitation-contraction coupling. *Nature.* 415:198–205. https://doi.org/10.1038/415198a

Bers, D.M. 2012. Ryanodine receptor S2808 phosphorylation in heart failure: smoking gun or red herring. *Circ. Res.* 110:796–799. https://doi.org/10.1161/CIRCRESAHA.112.265579

Blayney, L.M., and F.A. Lai. 2009. Ryanodine receptor-mediated arrhythmias and sudden cardiac death. *Pharmacol. Ther.* 123:151–177. https://doi.org/10.1016/j.pharmthera.2009.03.006

Bovo, E., S. Huke, L.A. Blatter, and A.V. Zima. 2017. The effect of PKA-mediated phosphorylation of ryanodine receptor on SR Ca^{2+} leak in ventricular myocytes. *J. Mol. Cell. Cardiol.* 104:9–16. https://doi.org/10.1016/j.yjmcc.2017.01.015

Camors, E., and H.H. Valdivia. 2014. CaMKII regulation of cardiac ryanodine receptors and inositol triphosphate receptors. *Front. Pharmacol.* 5:101. https://doi.org/10.3389/fphar.2014.00101

Cannell, M.B., C.H.T. Kong, M.S. Imtiaz, and D.R. Laver. 2013. Control of sarcoplasmic reticulum Ca^{2+} release by stochastic RyR gating within a 3D model of the cardiac dyad and importance of induction decay for CICR termination. *Biophys. J.* 104:2149–2159. https://doi.org/10.1016/j.bpj.2013.03.058

Chan, Y.-H., W.-C. Tsai, Z. Song, C.Y. Ko, Z. Qu, J.N. Weiss, S.-F. Lin, P.-S. Chen, L.R. Jones, and Z. Chen. 2015. Acute reversal of phospholamban inhibition facilitates the rhythmic whole-cell propagating calcium waves in isolated ventricular myocytes. *J. Mol. Cell. Cardiol.* 80:126–135. https://doi.org/10.1016/j.yjmcc.2014.12.024

Dries, E., D.J. Santiago, D.M. Johnson, G. Gilbert, P. Holemans, S.M. Korte, H.L. Roderick, and K.R. Sipido. 2016. Calcium/calmodulin-dependent kinase II and nitric oxide synthase 1-dependent modulation of ryanodine receptors during β-adrenergic stimulation is restricted to the dyadic cleft. *J. Physiol.* 594:5923–5939. https://doi.org/10.1113/JP271965

Fischer, T.H., J. Herting, T. Tirilomis, A. Renner, S. Neef, K. Toischer, D. Ellenberger, A. Förster, J.D. Schmitto, J. Gummert, et al. 2013. Ca^{2+}/calmodulin-dependent protein kinase II and protein kinase A differentially regulate sarcoplasmic reticulum Ca^{2+} leak in human cardiac pathology. *Circulation.* 128:970–981. https://doi.org/10.1161/CIRCULATIONAHA.113.001746

George, C.H., H. Jundi, N.L. Thomas, D.L. Fry, and F.A. Lai. 2007. Ryanodine receptors and ventricular arrhythmias: emerging trends in mutations, mechanisms and therapies. *J. Mol. Cell. Cardiol.* 42:34–50. https://doi.org/10.1016/j.yjmcc.2006.08.115

Ginsburg, K.S., and D.M. Bers. 2004. Modulation of excitation-contraction coupling by isoproterenol in cardiomyocytes with controlled SR Ca^{2+} load and Ca^{2+} current trigger. *J. Physiol.* 556:463–480. https://doi.org/10.1113/jphysiol.2003.055384

Gutierrez, D.A., M. Fernandez-Tenorio, J. Ogrodnik, and E. Niggli. 2013. NO-dependent CaMKII activation during β-adrenergic stimulation of cardiac muscle. *Cardiovasc. Res.* 100:392–401. https://doi.org/10.1093/cvr/cvt201

Hartmann, N., S. Pabel, J. Herting, F. Schatter, A. Renner, J. Gummert, H. Schotola, B.C. Danner, L.S. Maier, N. Frey, et al. 2017. Antiarrhythmic effects of dantrolene in human diseased cardiomyocytes. *Heart Rhythm.* 14:412–419. https://doi.org/10.1016/j.hrthm.2016.09.014

Hilliard, F.A., D.S. Steele, D. Laver, Z. Yang, S.J. Le Marchand, N. Chopra, D.W. Piston, S. Huke, and B.C. Knollmann. 2010. Flecainide inhibits arrhythmogenic Ca^{2+} waves by open state block of ryanodine receptor Ca^{2+} release channels and reduction of Ca^{2+} spark mass. *J. Mol. Cell. Cardiol.* 48:293–301. https://doi.org/10.1016/j.yjmcc.2009.10.005

Huke, S., and D.M. Bers. 2008. Ryanodine receptor phosphorylation at Serine 2030, 2808 and 2814 in rat cardiomyocytes. *Biochem. Biophys. Res. Commun.* 376:80–85. https://doi.org/10.1016/j.bbrc.2008.08.084

Jones, P.P., X. Meng, B. Xiao, S. Cai, J. Bolstad, T. Wagenknecht, Z. Liu, and S.R.W. Chen. 2008. Localization of PKA phosphorylation site, Ser(2030), in the three-dimensional structure of cardiac ryanodine receptor. *Biochem. J.* 410:261–270. https://doi.org/10.1042/BJ20071257

Li, Y., E.G. Kranias, G.A. Mignery, and D.M. Bers. 2002. Protein kinase A phosphorylation of the ryanodine receptor does not affect calcium sparks in mouse ventricular myocytes. *Circ. Res.* 90:309–316. https://doi.org/10.1161/hh0302.105660

Louch, W.E., K.A. Sheehan, and B.M. Wolska. 2011. Methods in cardiomyocyte isolation, culture, and gene transfer. *J. Mol. Cell. Cardiol.* 51:288–298. https://doi.org/10.1016/j.yjmcc.2011.06.012

Marx, S.O., S. Reiken, Y. Hisamatsu, T. Jayaraman, D. Burkhoff, N. Rosemblit, and A.R. Marks. 2000. PKA phosphorylation dissociates FKBP12.6 from the calcium release channel (ryanodine receptor): defective regulation in failing hearts. *Cell.* 101:365–376. https://doi.org/10.1016/S0092-8674(00)80847-8

Niggli, E., N.D. Ullrich, D. Gutierrez, S. Kyrychenko, E. Poláková, and N. Shirokova. 2013. Posttranslational modifications of cardiac ryanodine receptors: Ca^{2+} signaling and EC-coupling. *Biochim. Biophys. Acta.* 1833:866–875. https://doi.org/10.1016/j.bbamcr.2012.08.016

Ogrodnik, J., and E. Niggli. 2010. Increased Ca^{2+} leak and spatiotemporal coherence of Ca^{2+} release in cardiomyocytes during β-adrenergic stimulation. *J. Physiol.* 588:225–242. https://doi.org/10.1113/jphysiol.2009.181800

Pereira, L., G. Ruiz-Hurtado, E. Morel, A.-C. Laurent, M. Métrich, A. Domínguez-Rodríguez, S. Lauton-Santos, A. Lucas, J.-P. Benitah, D.M. Bers, et al. 2012. Epac enhances excitation-transcription coupling in cardiac my-

ocytes. *J. Mol. Cell. Cardiol.* 52:283–291. https://doi.org/10.1016/j.yjmcc.2011.10.016

Picht, E., A.V. Zima, L.A. Blatter, and D.M. Bers. 2007. SparkMaster: automated calcium spark analysis with ImageJ. *Am. J. Physiol. Cell Physiol.* 293:C1073–C1081. https://doi.org/10.1152/ajpcell.00586.2006

Poláková, E., A. Illaste, E. Niggli, and E.A. Sobie. 2015. Maximal acceleration of Ca^{2+} release refractoriness by β-adrenergic stimulation requires dual activation of kinases PKA and CaMKII in mouse ventricular myocytes. *J. Physiol.* 593:1495–1507. https://doi.org/10.1113/jphysiol.2014.278051

Priori, S.G., and S.R.W. Chen. 2011. Inherited dysfunction of sarcoplasmic reticulum Ca^{2+} handling and arrhythmogenesis. *Circ. Res.* 108:871–883. https://doi.org/10.1161/CIRCRESAHA.110.226845

Ramay, H.R., O.Z. Liu, and E.A. Sobie. 2011. Recovery of cardiac calcium release is controlled by sarcoplasmic reticulum refilling and ryanodine receptor sensitivity. *Cardiovasc. Res.* 91:598–605. https://doi.org/10.1093/cvr/cvr143

Respress, J.L., R.J. van Oort, N. Li, N. Rolim, S.S. Dixit, A. deAlmeida, N. Voigt, W.S. Lawrence, D.G. Skapura, K. Skårdal, et al. 2012. Role of RyR2 phosphorylation at S2814 during heart failure progression. *Circ. Res.* 110:1474–1483. https://doi.org/10.1161/CIRCRESAHA.112.268094

Shan, J., M.J. Betzenhauser, A. Kushnir, S. Reiken, A.C. Meli, A. Wronska, M. Dura, B.-X. Chen, and A.R. Marks. 2010. Role of chronic ryanodine receptor phosphorylation in heart failure and β-adrenergic receptor blockade in mice. *J. Clin. Invest.* 120:4375–4387. https://doi.org/10.1172/JCI37649

Sikkel, M.B., D.P. Francis, J. Howard, F. Gordon, C. Rowlands, N.S. Peters, A.R. Lyon, S.E. Harding, and K.T. MacLeod. 2017. Hierarchical statistical techniques are necessary to draw reliable conclusions from analysis of isolated cardiomyocyte studies. *Cardiovasc. Res.* 113:1743–1752. https://doi.org/10.1093/cvr/cvx151

Sobie, E.A., K.W. Dilly, J. dos Santos Cruz, W.J. Lederer, and M.S. Jafri. 2002. Termination of cardiac Ca^{2+} sparks: an investigative mathematical model of calcium-induced calcium release. *Biophys. J.* 83:59–78. https://doi.org/10.1016/S0006-3495(02)75149-7

Sobie, E.A., L.-S. Song, and W.J. Lederer. 2005. Local recovery of Ca^{2+} release in rat ventricular myocytes. *J. Physiol.* 565:441–447. https://doi.org/10.1113/jphysiol.2005.086496

Ullrich, N.D., H.H. Valdivia, and E. Niggli. 2012. PKA phosphorylation of cardiac ryanodine receptor modulates SR luminal Ca^{2+} sensitivity. *J. Mol. Cell. Cardiol.* 53:33–42. https://doi.org/10.1016/j.yjmcc.2012.03.015

Valdivia, H.H. 2012. Ryanodine receptor phosphorylation and heart failure: phasing out S2808 and "criminalizing" S2814. *Circ. Res.* 110:1398–1402. https://doi.org/10.1161/CIRCRESAHA.112.270876

van Oort, R.J., M.D. McCauley, S.S. Dixit, L. Pereira, Y. Yang, J.L. Respress, Q. Wang, A.C. De Almeida, D.G. Skapura, M.E. Anderson, et al. 2010. Ryanodine receptor phosphorylation by calcium/calmodulin-dependent protein kinase II promotes life-threatening ventricular arrhythmias in mice with heart failure. *Circulation.* 122:2669–2679. https://doi.org/10.1161/CIRCULATIONAHA.110.982298

Wehrens, X.H.T., S.E. Lehnart, S.R. Reiken, and A.R. Marks. 2004. Ca^{2+}/calmodulin-dependent protein kinase II phosphorylation regulates the cardiac ryanodine receptor. *Circ. Res.* 94:e61–e70. https://doi.org/10.1161/01.RES.0000125626.33738.E2

Wehrens, X.H.T., S.E. Lehnart, S. Reiken, J.A. Vest, A. Wronska, and A.R. Marks. 2006. Ryanodine receptor/calcium release channel PKA phosphorylation: a critical mediator of heart failure progression. *Proc. Natl. Acad. Sci. USA.* 103:511–518. https://doi.org/10.1073/pnas.0510113103

Willis, B.C., S.V. Pandit, D. Ponce-Balbuena, M. Zarzoso, G. Guerrero-Serna, B. Limbu, M. Deo, E. Camors, R.J. Ramirez, S. Mironov, et al. 2016. Constitutive intracellular Na^{+} excess in Purkinje cells promotes arrhythmogenesis at lower levels of stress than ventricular myocytes from mice with catecholaminergic polymorphic ventricular tachycardia. *Circulation.* 133:2348–2359. https://doi.org/10.1161/CIRCULATIONAHA.116.021936

Witcher, D.R., R.J. Kovacs, H. Schulman, D.C. Cefali, and L.R. Jones. 1991. Unique phosphorylation site on the cardiac ryanodine receptor regulates calcium channel activity. *J. Biol. Chem.* 266:11144–11152.

Xiao, B., M.T. Jiang, M. Zhao, D. Yang, C. Sutherland, F.A. Lai, M.P. Walsh, D.C. Warltier, H. Cheng, and S.R.W. Chen. 2005. Characterization of a novel PKA phosphorylation site, serine-2030, reveals no PKA hyperphosphorylation of the cardiac ryanodine receptor in canine heart failure. *Circ. Res.* 96:847–855. https://doi.org/10.1161/01.RES.0000163276.26083.e8

Xiao, B., X. Tian, W. Xie, P.P. Jones, S. Cai, X. Wang, D. Jiang, H. Kong, L. Zhang, K. Chen, et al. 2007. Functional consequence of protein kinase A-dependent phosphorylation of the cardiac ryanodine receptor: sensitization of store overload-induced Ca^{2+} release. *J. Biol. Chem.* 282:30256–30264. https://doi.org/10.1074/jbc.M703510200

Yuchi, Z., K. Lau, and F. Van Petegem. 2012. Disease mutations in the ryanodine receptor central region: crystal structures of a phosphorylation hot spot domain. *Structure.* 20:1201–1211. https://doi.org/10.1016/j.str.2012.04.015

Zhang, H., C.A. Makarewich, H. Kubo, W. Wang, J.M. Duran, Y. Li, R.M. Berretta, W.J. Koch, X. Chen, E. Gao, et al. 2012. Hyperphosphorylation of the cardiac ryanodine receptor at serine 2808 is not involved in cardiac dysfunction after myocardial infarction. *Circ. Res.* 110:831–840. https://doi.org/10.1161/CIRCRESAHA.111.255158

Supplemental material

Potenza et al., https://doi.org/10.1085/jgp.201812155

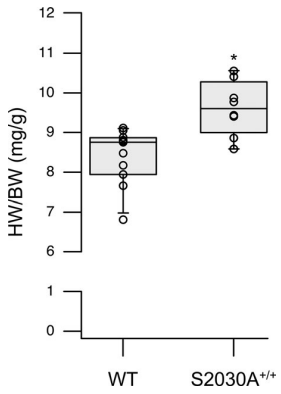

Figure S1. **S2030A$^{+/+}$ display a higher HW/BW ratio compared with WT animals.** HW/BW ratio was measured and used as an index of hypertrophy (see Materials and methods for details; WT: N = 11; 31.25 ± 1.07 g [BW]; 262 ± 8 mg [HW]; 8.41 ± 0.21 [HW/BW]; S2030A$^{+/+}$: *N* = 8; 32.45 ± 0.86 g [BW]; 311 ± 9 mg [HW]; 9.61 ± 0.24 [HW/BW]). The data are expressed as mean ± SEM of all measurements. *, P < 0.05 versus WT. The whiskers cover the range from 10% to 90%.

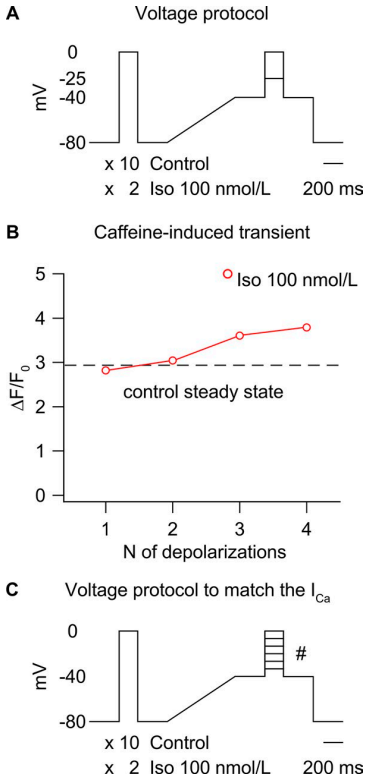

Figure S2. **Recording protocols. (A)** Myocytes were held at a potential of −80 mV, and an initial step to −40 mV was applied to inactivate Na^+ and T-type Ca^{2+} currents. For each cell, peak Ca^{2+} current was then measured at two membrane potentials (from −40 to −25 mV and −40 to 0 mV) in control and during subsequent Iso application. The extent of SR Ca^{2+} loading in a single cell was controlled under whole-cell patch-clamp conditions by using a train with a different number of depolarization steps (10 for control and 2 for Iso) of 200-ms duration at 0.5 Hz. **(B)** The train of depolarizations was preceded by a rapid caffeine exposure in order to reset SR Ca^{2+} content, and the steady-state in control was achieved after 10 depolarization steps. In Iso, after the initial caffeine application, the SR was reloaded with one, two, three, and four depolarizations. We estimated the SR Ca^{2+} content from the peak amplitude of the caffeine-induced transient ($\Delta F/F_0$), and we compared control steady state and Iso at an increasing number of stimulations. The amplitude after two depolarizations in Iso was the closest value to control, and it was used to match the control SR Ca^{2+} content. A cell was considered for analysis when the difference between control and Iso SR Ca^{2+} load was within ±15% (>75% of the patched myocytes). The cells that did not meet the criteria were excluded. **(C)** To compare the ECC gain in myocytes with similar SR Ca^{2+} load and similar I_{Ca}, additional recordings were performed for both WT and S2030A$^{+/+}$ animals. Starting from the same loading protocol shown in A, the cells were selected according to their SR Ca^{2+} content (mean WT ±15%). For these measurements, the I_{Ca} trigger was also maintained constant between groups using a recording protocol with variously sized I_{Ca}. After the conditioning step, six currents (#) were recorded, from −40 to −25 mV up to 0 mV (+5-mV steps) in control and from −40 to −35 mV up to −10 mV for Iso. In Iso, an extra recording was performed with a different range of I_{Ca} trigger (from −40 to −30 mV up to −15 mV, with +3-mV steps). Between the recorded currents, a matching pair was selected per each cell (WT and mutant) considering the mean WT I_{Ca} (±15%). A cell was considered for analysis when the difference between the I_{Ca} in control and Iso was within ±15%. The cells that did not meet the criteria were excluded.

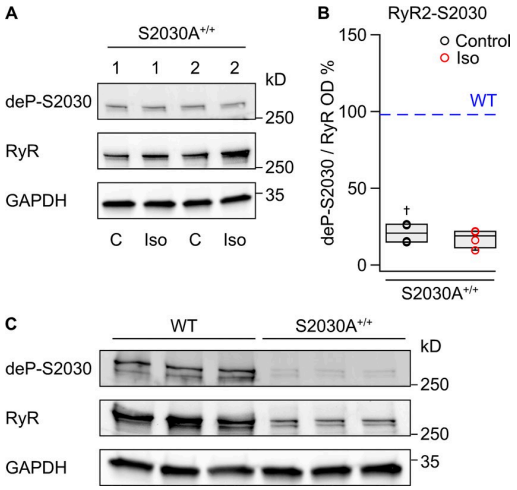

Figure S3. **Iso treatment does not change the dephospho-RyR2-S2030/RyR fraction in RyR2-S2030A$^{+/+}$ cells. (A)** Representative Western blot showing the signal generated by the dephospho-RyR2-S2030 Ab in myocytes isolated from S2030A$^{+/+}$ animals (N = 4) before (C, control) and after application of 100 nmol/liter Iso. The numbers 1 and 2 identify different animals. Numbers on the right (250 and 35 kDa) refer to the protein ladder. **(B)** The dephospho-RyR2-S2030/RyR ratio was significantly lower compared with WT. The dashed blue line represents the median of the WT dephospho-RyR2-S2030/RyR fraction reported in Fig. 2. In contrast to WT, the signal was not modified by Iso confirming, indirectly, the ablation of the phosphorylation site. The level of the phosphorylation was expressed as ratio of the dephospho-RyR2-S2030 and the anti-RyR Ab OD, both normalized to the GAPDH signal. There are two possible reasons for the low signal detected by the dephospho-Ab in S2030A$^{+/+}$ cells: (1) there is less RyR2 expression in S2030A$^{+/+}$ cells, and (2) the dephospho-Ab (designed to recognize the dephospho-S2030 site in WT) weakly binds the epitope with the alanine substitution (S2030A$^{+/+}$), which suggests specificity of the dephospho-Ab for the S2030 site. **(C)** Blot showing comparison between WT and S2030A$^{+/+}$ cells. †, $P < 0.05$ S2030A$^{+/+}$ versus WT. The whiskers cover the range from 10% to 90%.

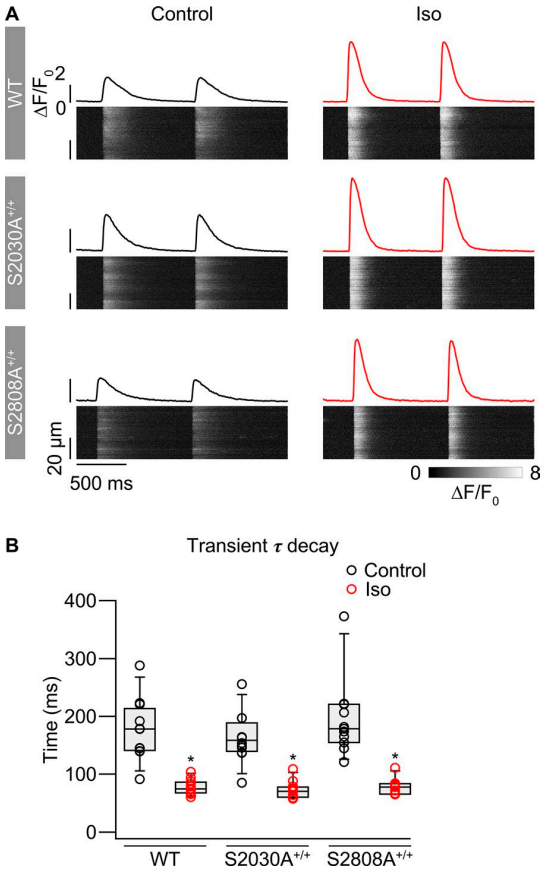

Figure S4. **Acceleration of the time course of the Ca^{2+} transient decay by Iso.** The cells were electrically stimulated at 1 Hz for 30 s. **(A)** Representative line profiles of the Ca^{2+} transients as relative changes in cytosolic Ca^{2+} concentrations ($\Delta F/F_0$; black traces for the control and red for Iso) and the corresponding confocal line-scan images for WT, S2030A$^{+/+}$, and S2808A$^{+/+}$ fluo-3 AM–loaded myocytes. **(B)** τ decay of Ca^{2+} transients before and after Iso application for WT (N = 4, *n* = 12), S2030A$^{+/+}$ (N = 4, *n* = 13), and S2808A$^{+/+}$ (N = 3, *n* = 10) myocytes. The amplitude of the Ca^{2+} transients in control and Iso were comparable between the animals (Bers and Berlin, 1995). *, P < 0.05 versus control. The whiskers cover the range from 10% to 90%.

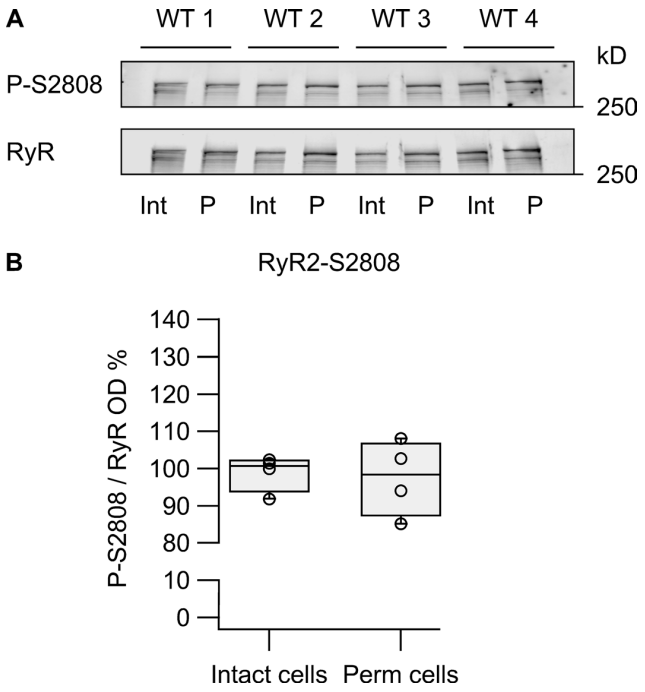

Figure S5. **β-escin permeabilization does not change phosphorylation at the RyR2-S2808 site. (A)** Western blot showing the level of RyR2-S2808 site phosphorylation before (intact cells [Int]) and after (permeabilized cells [P]) 20 min from the cells' permeabilization with β-escin. In the gel, samples from four different WT animals were run simultaneously. The 250 (kDa) label indicates the molecular weight of the protein ladder. **(B)** The level of phosphorylation was expressed as ratio of the anti-phospho-RyR2-S2808 and the total-RyR signals (OD). *, $P < 0.05$ versus intact cells. The whiskers cover the range from 10% to 90%.

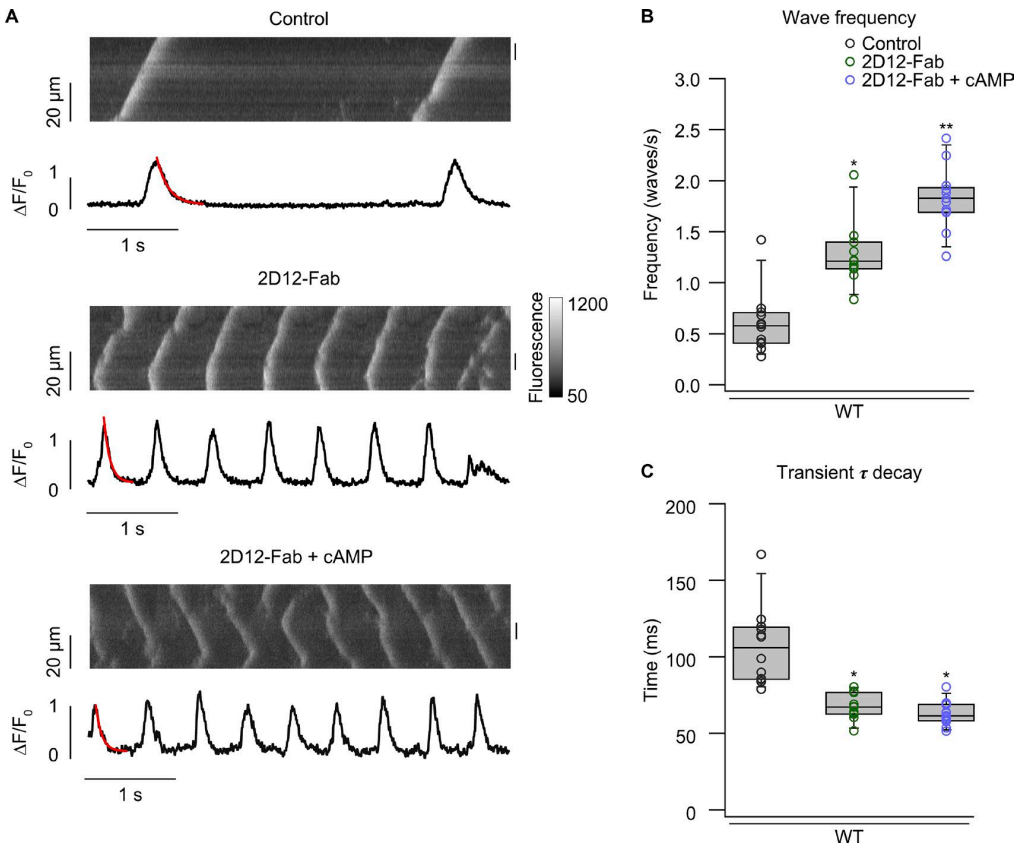

Figure S6. **cAMP does not further accelerate SERCA activity in 2D12-Fab–treated cells. (A)** Representative line scans and line profiles recorded in permeabilized cells before and after treatment with 100 µg/ml 2D12-Fab (15 min) and 20 µmol/liter cAMP. A monoexponential function was used to fit (red lines) the decreasing phase of the Ca^{2+} waves and measure the τ decay, reflecting SR Ca^{2+} pump activity. **(B)** Application of the 2D12-Fab fragment increased the frequency of Ca^{2+} release events. The frequency was further increased after cAMP application (5 min). **(C)** The τ decay was significantly faster in cells treated with the antibody (N = 3, *n* = 11) than in untreated cells (N = 3, *n* = 12), indicating a faster activity of the SERCA pump. Further cAMP application (N = 3, *n* = 14) did not accelerate the decay, suggesting an already fully activated SERCA. *, P < 0.05 versus control; **, P < 0.05 versus 2D12-Fab. The whiskers cover the range from 10% to 90%.

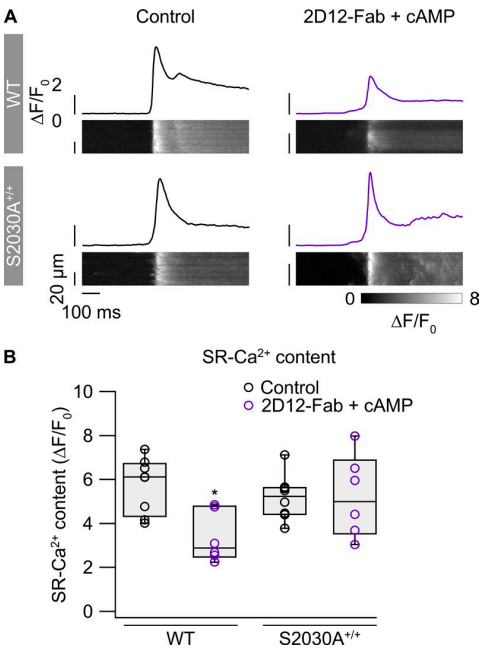

Figure S7. **cAMP decreases SR Ca^{2+} content in 2D12-Fab–treated WT cells. (A)** Representative line-scan images and line profiles of 20 mmol/liter caffeine-dependent Ca^{2+} transients recorded in control and after 2D12-Fab/cAMP combined treatment. **(B)** SR Ca^{2+} content is estimated from the amplitude of the caffeine-transient (expressed as $\Delta F/F_0$). After treatment with the 2D12-Fab fragment, cAMP reduced SR Ca^{2+} content in WT cells, but not in S2030A$^{+/+}$ cells, mirroring the observation of cAMP-induced Ca^{2+} sparks exclusively in WT cells (see Fig. 4; N = 3, *n* = 8 for control and *n* = 6 for 2D12-Fab + cAMP for both animals). *, P < 0.05 versus control. The whiskers cover the range from 10% to 90%.

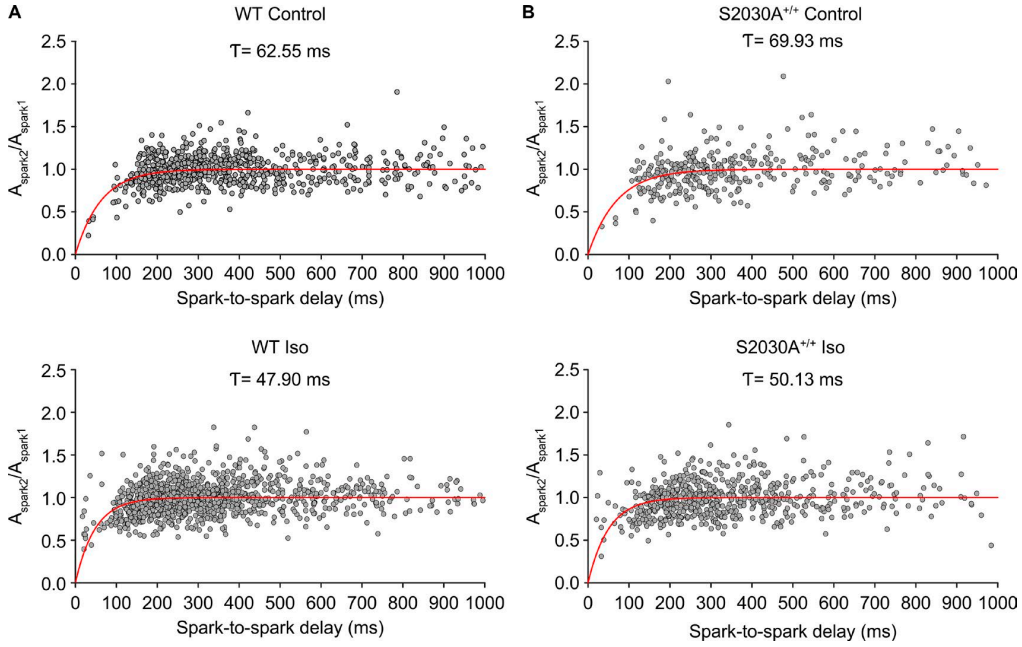

Figure S8. **Spark amplitude restitution. (A and B)** Spark amplitude restitution for WT (A) and S2030A$^{+/+}$ (B) myocytes at control conditions and during β-adrenergic stimulation with 100 nmol/liter Iso. Each plot shows the normalized amplitude of the second spark (A_{spark2}/A_{spark1}) versus the delay between sparks. Spark amplitude ratios were fitted with a single exponential curve (red line; control WT: 62.55 ms, 95% CI, 54.24–70.85 ms, N = 10, *n* = 35, 749 spark pairs; Iso WT: 47.90 ms, 95% CI, 41.65–54.14 ms, N = 11, *n* = 43, 1,196 spark pairs; control S2030A$^{+/+}$: 69.93 ms, 95% CI, 57.59–82.26 ms, N = 6, *n* = 20, 380 spark pairs; Iso S2030A$^{+/+}$: 50.13 ms, 95% CI, 41.38–58.87 ms, N = 7, *n* = 27, 689 spark pairs).

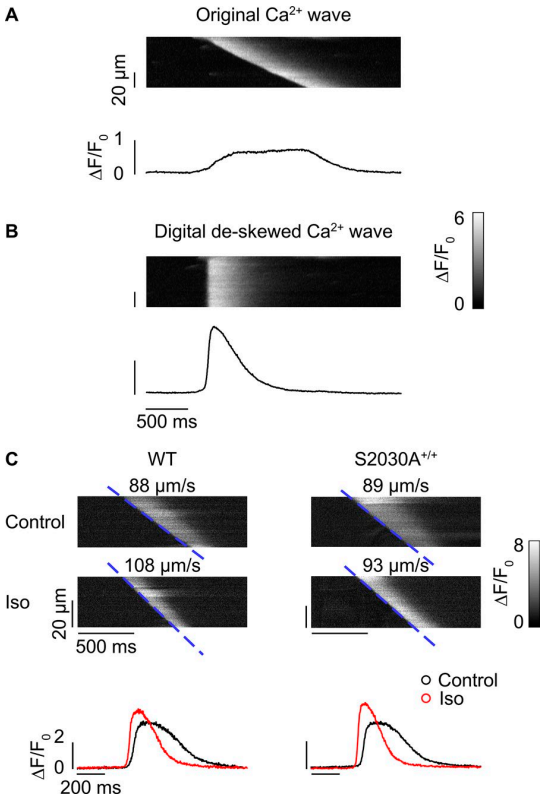

Figure S9. **Ca^{2+} wave analysis.** To evoke the waves, we elevated the extracellular Ca^{2+} concentration to 10 mmol/liter, which resulted in SR Ca^{2+} overload. **(A)** Representative line-scan image and the corresponding line profile of a Ca^{2+} wave induced by high $[Ca^{2+}]_o$. The global line profile did not allow an accurate measurement of the time course of the Ca^{2+} signal. **(B)** The Ca^{2+} wavefront has been aligned by digital deskewing, and the related line profile was used to measure the τ decay of the Ca^{2+} signal (representative of SERCA pump activity). **(C)** Representative line-scan images and line profiles of Ca^{2+} waves measured in WT and S2030A$^{+/+}$ myocytes. The profiles clearly show that SERCA is stimulated by Iso in both cell types (red traces display a faster decreasing phase). Note the differences in the angle of the wavefront (indicated by the blue dashed lines) between WT and S2030A$^{+/+}$ during Iso treatment.

Table S1. **Statistical summary of the echocardiograph measurements**

	Fractional shortening (%)	LV volume diastole (µl)	LV volume systole (µl)	LV B-mode LV ejection fraction (µl)	LV B-mode LV volume (µl)	LV B-mode stroke volume (µl)
WT (N = 7)	31.9 ± 2.0	62.2 ± 4.1	22.3 ± 1.8	57.4 ± 1.4	41.2 ± 2.5	28.2 ± 0.5
S2030A (N = 7)	36.1 ± 4.3	74.4 ± 6	29.0 ± 7	62.9 ± 5.8	42.5 ± 3.5	31.3 ± 2.3

Mice at the age of 3 mo were anesthetized with 5% isoflurane inhalation and maintained in the anesthetized state by 1.5–2% isoflurane. Two-dimensionally guided B-mode imaging was used to measure the LV volume during systole and diastole, the stroke volume, and the ejection fraction. The fractional shortening was also calculated using the formula: [(LV diameter diastole − LV diameter systole)/LV diameter diastole] × 100. The LV diastolic and systolic volume and the fractional shortening and ejection fraction were slightly increased in S2030A$^{+/+}$ animals compared to WT animals, but none of the observed differences was statistically significant (all $P > 0.05$).

Table S2. **Statistical summary of the Ca^{2+} transient amplitude at matched I_{Ca} and SR Ca^{2+} load**

	Matched I_{Ca}	Measured transient amplitude	Matched SR Ca^{2+} content
	(pA/pF)	($\Delta F/F_0$)	($\Delta F/F_0$)
WT (N = 3/*n* = 8)			
Control	2.75 ± 0.07	2.27 ± 0.25	2.80 ± 0.11
Iso	2.80 ± 0.12	2.15 ± 0.18	2.88 ± 0.06
S2030A (N = 4/*n* = 6)			
Control	3.09 ± 0.15	2.13 ± 0.29	2.72 ± 0.09
Iso	3.05 ± 0.12	0.90 ± 0.16[a,b]	2.71 ± 0.14

Using the protocol described in Fig. S2, the SR Ca^{2+} content (measured as the amplitude of the caffeine-evoked transients) was experimentally matched between control and Iso in all cells. We reported a difference in the SR Ca^{2+} load between WT and mutant myocytes (Fig. 1). To further compare WT and S2030A$^{+/+}$ cells, we assessed the ECC gain in conditions of matched SR Ca^{2+} load and matched I_{Ca} between all the groups (see Fig. S2 for details). In these experimental conditions, the Ca^{2+} release in WT myocytes did not change during Iso. However, the Ca^{2+} release was decreased in S2030A$^{+/+}$ after Iso application, corroborating the conclusion that the S2030 site may be involved in RyR2 sensitization during the β-adrenergic response. Data are expressed as means ± SEM of *n* measurements.
[a]P < 0.05 versus control.
[b]P < 0.05 versus WT.

Table S3. **Statistical summary of the Ca^{2+} spark parameters**

	Frequency	Amplitude	FWHM	FDHM	Spark mass
	(sparks/100 µm/s)	($\Delta F/F_0$)	(µm)	(ms)	($\Delta F/F_0 \times \mu m^3$)
WT (N = 4/*n* = 12)					
Control	0.32 ± 0.08	1.10 ± 0.15	2.11 ± 0.12	36.75 ± 2.99	14.51 ± 2.32
Iso	1.95 ± 0.29[a]	1.59 ± 0.15[a]	2.18 ± 0.12	36.59 ± 2.83	38.97 ± 13.19[a]
S2030A (N = 4/*n* = 13)					
Control	0.37 ± 0.07	1.01 ± 0.08	2.09 ± 0.19	36.81 ± 3.49	14.48 ± 4.68
Iso	1.05 ± 0.15[a,b]	1.08 ± 0.09[b]	1.97 ± 0.16	38.03 ± 2.52	15.51 ± 3.49[b]
S2808A (N = 3/*n* = 10)					
Control	0.33 ± 0.07	0.98 ± 0.16	2.14 ± 0.11	39.97 ± 7.46	12.72 ± 1.87
Iso	2.14 ± 0.33[a]	1.28 ± 0.18[a]	2.23 ± 0.18	42.43 ± 3.95	34.13 ± 11.36[a]

Spontaneous Ca^{2+} sparks were recorded in intact cells after a train of electrical stimulations at 1 Hz for 30 s (0.5-ms pulses at 20–40 V) and were quantified with the ImageJ plug-in SparkMaster. Spark mass was calculated as 1.206 × amplitude × FWHM^3. Data are expressed as means ± SEM of *n* measurements. FDHM, full duration at half maximum; FWHM, full width at half maximum.
[a]P < 0.05 versus control.
[b]P < 0.05 versus WT.

References

Bers, D.M., and J.R. Berlin. 1995. Kinetics of $[Ca]_i$ decline in cardiac myocytes depend on peak $[Ca]_i$. *Am. J. Physiol.* 268:C271–C277. https://doi.org/10.1152/ajpcell.1995.268.1.C271